International
Progress Report

IPR-01-40

Äspö Hard Rock Laboratory

Prototype Repository

Groundwater flow, pressure and salinity distributions around the Prototype Repository. Continuum model No 1

Urban Svensson
Computer-aided Fluid Engineering AB

November 2001

Svensk Kärnbränslehantering AB
Swedish Nuclear Fuel
and Waste Management Co
Box 5864
SE-102 40 Stockholm Sweden
Tel +46 8 459 84 00
Fax +46 8 661 57 19

Äspö Hard Rock
Laboratory

Report no.
IPR-01-40
No.
F63K
Author
Urban Svensson
Date
01-11-08
Checked by
Ingvar Rhen, VBB VIAK
Date
01-11-10
Approved
Christer Svemar
Date
01-12-06

Äspö Hard Rock Laboratory

Prototype Repository

Groundwater flow, pressure and salinity distributions around the Prototype Repository. Continuum model No 1

Urban Svensson
Computer-aided Fluid Engineering AB

November 2001

Keywords: Äspö HRL, Prototype Repository, groundwater, flow, salinty, continuum model, Äspö

FOREWORD

This report summarises the results from two SKB projects: Modelling techniques and Groundwater Flow Modelling of the Prototype Repository, with a continuum approach. The first project was mainly concerned with development of new methods and techniques, while the second project can be characterised as an application of these developments.

ABSTRACT

The objective of this study is to develop, calibrate and apply a numerical simulation model of the Prototype Repository part of the Äspö Hard Rock Laboratory (HRL). The work is part of a project called “The Prototype Repository Project”, which aims to test important components in SKB´s deep repository system, in full scale and in a realistic environment. It is further the objective to deliver data files of the simulation results; files which are intended to be used in other modelling studies.

A calibration study demonstrates that the numerical model can describe the pressure distribution around the Prototype Repository in a realistic manner. Five realisations of the conductivity fields are used to show the sensitivity to different background fracture networks. In the Result section the pressure and salinity fields that result from the five realisations are illustrated and discussed.
The main conclusion of the study is that the five realisations of the hydraulic conductivity field generate realistic distributions of pressure and salinity (although the salinity fields were not directly compared with field data).

ABSTRACT (Swedish)

Syftet med studien är att utveckla, kalibrera och tillämpa en numerisk simuleringsmodell för Prototypförvarsexperimentet. Detta experiment ingår i sin tur i SKB:s experimentprogram för att testa olika komponenter i SKB:s djupförvarssystem. Projektet syftar vidare till att generera en serie datafiler, av tryck och salt fördelningen runt Prototypförvaret. Dessa datafiler är avsedda att ge rand- och initialvärden för andra modellstudier av Prototypförvaret.

En kalibreringsstudie visar att den numeriska modellen beskriver tryckfördelningen runt Prototypförvaret på ett acceptabelt sätt. Fem realiseringar av det hydrauliska konduktivitetsfältet används för att studera känsligheten med avseende på det stokastiska fältet av bakgrundssprickor. I resultatsektionen av rapporten illustreras och diskuteras tryck- och salinitetsfälten.
Den huvudsakliga slutsatsen från arbetet är att de fem realiseringarna av konduktivitetsfältet genererar realistiska tryck och salthaltsfördelningar runt Prototypförvaret.

TABLE OF CONTENTS

1 INTRODUCTION

1.1 BACKGROUND

The Äspö Hard Rock Laboratory (HRL) is an underground research facility which forms an important part of the Swedish programme for disposal of spent nuclear fuel in a fractured crystalline bedrock. Äspö was chosen because it represents geologically a variety of typical crystalline bedrock environments, both in terms of lithology and hydrostructural properties. The main objectives of the Äspö programme are to: 1) verify pre-investigation methods (i.e. surface and subsurface studies, mostly from boreholes), 2) finalise detailed characterisation methodology for future transfer to site-specific studies of candidate sites, 3) test models for groundwater flow and radionuclide retention (repository scale), 4) demonstrate repository design, construction and handling methods, and 5) test important parts of the repository system with respect to the long-term performance and safety of a deep disposal system for radioactive waste.

This report deals with a project called "The Prototype Repository Project", which is a part of the general programme outlined above. The aim of this project is to test important components in SKB:s deep repository system, in full scale and in a realistic environment. For further details about the project, see Dahlström (1997).

In the safety assessment of a deep repository for spent nuclear fuel, it is expected that numerical simulation models will play an important role. The models can provide estimates of the groundwater flow around the repository and transport times, from the repository to the biosphere, for radioactive spieces. One of the problems when setting up such models concerns scales. We need to consider length scales from 10 metres (canister performance) to a regional scale of perhaps 10 km. Most of the models have so far been set up for a site scale, which typically covers a volume of $1 \times 1 \times 1$ km^3. At the boundaries of a model one needs to make assumptions about the pressure and salinity distributions. The model to be presented in this report will derive boundary conditions from a Site scale model, see Svensson (1997b). The Site scale model employed boundary conditions from a Regional model, see Svensson (1997a); a model that covered a volume of 10 x 10 x 3 km^3. We thus have a systematic refinement, and generation of boundary conditions, from the regional scale to the finest scale resolved in the present Laboratory and Repository models, which is 1 metre.

1.2 SITE DESCRIPTION

The Äspö Hard Rock Laboratory is located near the Oskarshamn nuclear power plant on the east cost of Sweden, see Figure 1-1. The access tunnel starts on the mainland, continues under the Baltic and reaches the spiral part of the tunnel beneath the island of Äspö. The total length of the tunnel is 3600 metres and it reaches a depth of 450 metres below ground surface. A vertical elevator shaft connects the laboratory to the Äspö Research Village.

The horizontal extent of the Laboratory model is marked with a red rectangle in Figure 1-1. The depth interval considered is 200 to 560 metres. In Figure 1-1 a blue rectangle marks the model domain for the Prototype Repository. The depth interval is 412 to 488 metres for this domain. In the following we will call this domain the Repository model.

A more detailed view of the Prototype Repository area is given in Figure 1-2, where the six deposition holes as well as a number of boreholes are shown.

1.3 OBJECTIVES

The main objective of the study is to develop and establish an adequate model of the groundwater pressure and salinity distributions around the Prototype Repository. With “adequate model” it is understood that the model should be well balanced with respect to expected use, available data, scientific basis and computational resources.

More specifically the project should result in a set of three dimensional fields of pressure and salinity; fields that are intended to be used in other studies of the Prototype Repository. “Data delivery” is thus a key element of the work to be presented.

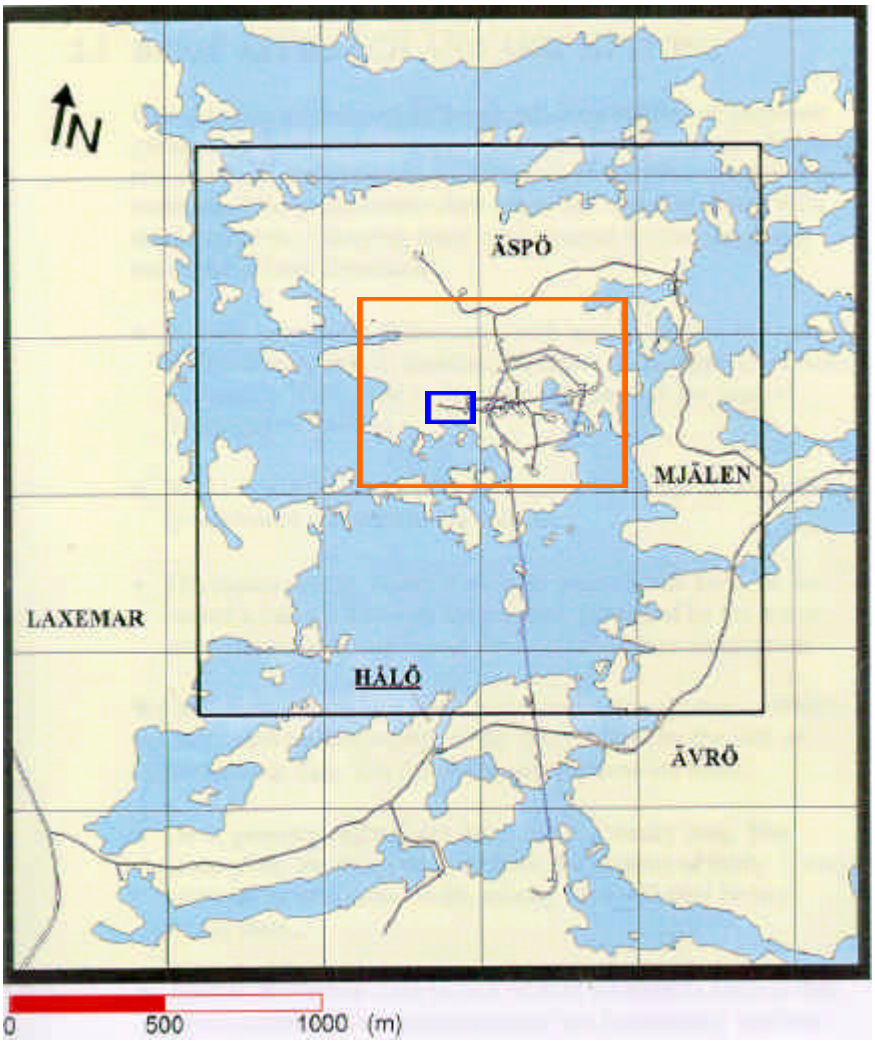

Figure 1-1. *The island of Äspö and the Äspö Hard Rock Laboratory. The black rectangle shows the area of the Site scale model, Svensson (1997b). The red rectangle shows the "coarse grid" computational domain, i.e. the Laboratory model, considered in this study. The blue rectangle indicates the domain for the Repository model.*

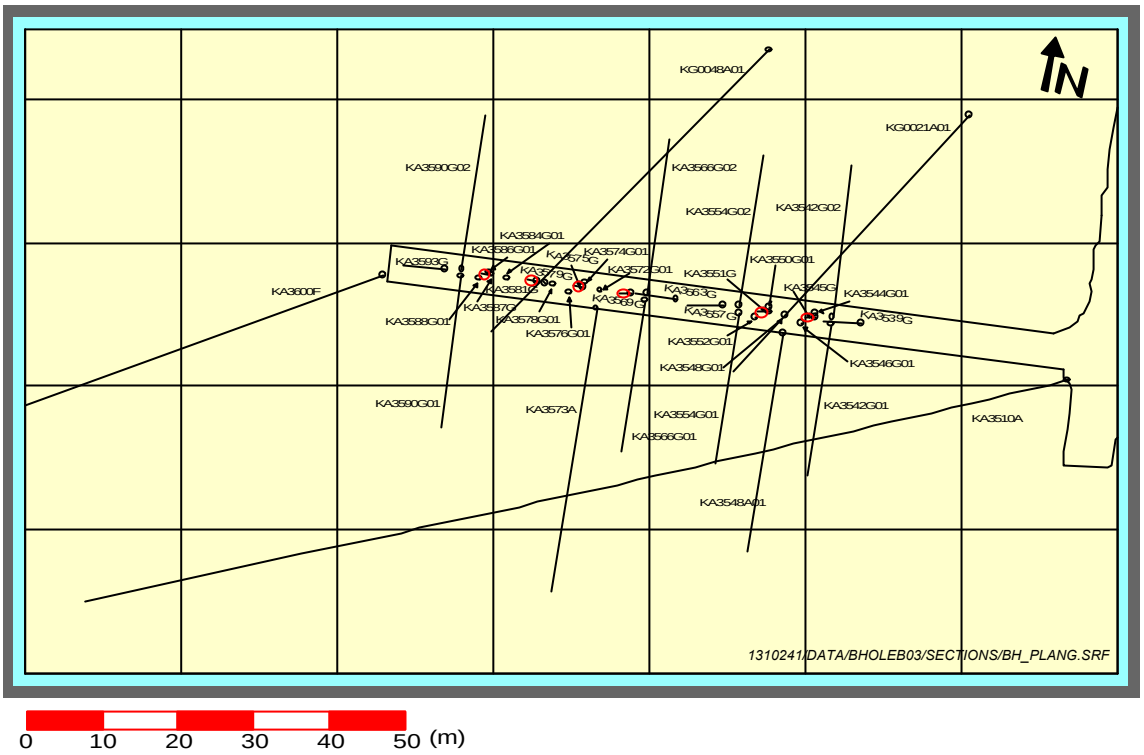

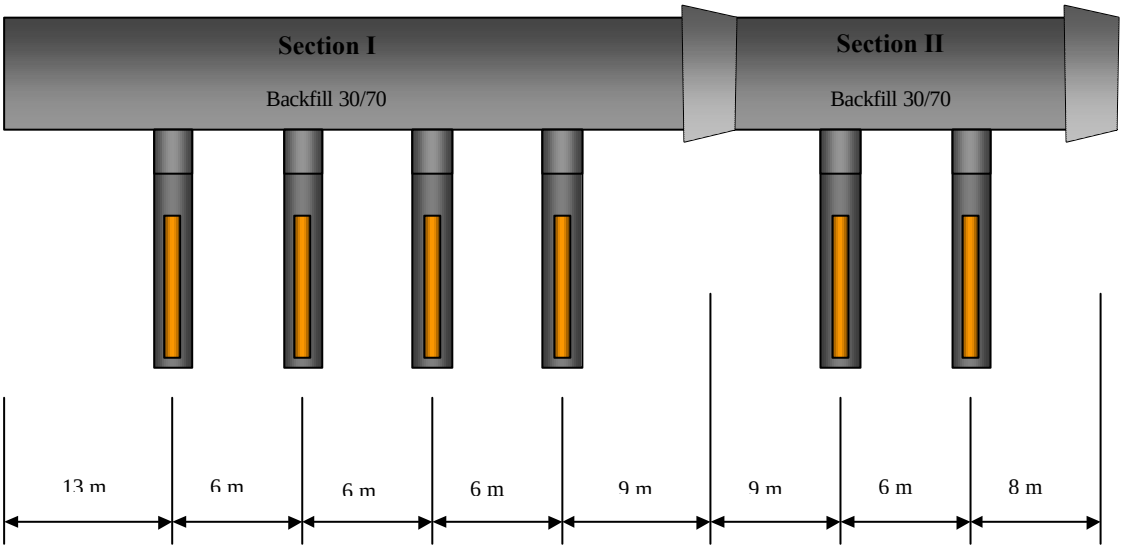

Figure 1-2. *The Prototype Repository area. Six deposition holes and boreholes used for pressure monitoring.*

2 BASIC CONCEPTUAL ASSUMPTIONS

2.1 INTRODUCTION

The numerical model to be used for the simulations can be described as "a continuum model based on a fracture network". The mathematical formulation of the model will be given in the next chapter; the basic concepts will however not be described in this report. A full account of the assumptions and concepts can be found in Svensson (1999a, b). Some of the main features will however be listed:

- Fracture intensity is specified from a power-law distribution.
- Fracture orientation is based on field data. Fracture sets are generated from a Fisher distribution.
- Fractures are assumed to be squares.
- Fracture properties (transmissivity, porosity, and aperture) are generated from semi-empirical relations.
- Major fracture zones are treated as deterministic features.

As mentioned, some further details will be given in the next chapter. In the rest of this chapter assumptions and concepts needed for the Prototype Repository simulations will be in focus; the following topics will be discussed: embedded grids, objectives of calibration and assumed conditions around the Prototype Repository.

2.2 EMBEDDED GRIDS

The Äspö HRL affects the pressure distribution within a large rock volume surrounding the laboratory. As the present task is to simulate the pressure levels, i.e. not drawdowns, in a volume around the Prototype Repository, it is realised that the large scale pressure response needs to be accounted for in some way. The approach to be adopted is outlined in Figure 2-1. The Repository and Laboratory models will be considered as fully coupled, i.e. solutions for the models are interacting. The Laboratory model receives boundary conditions from the Site model, now however without any coupling with the Site model; the same applies for the relation between the Regional model and the Site model. It is beyond the scope of the present report to discuss the various models mentioned, but it should be clear that the large scale pressure and salinity distributions are accounted for by the procedure outlined.

In the sequence of model runs outlined, it is the value of a variable (like pressure or salinity) that is transferred to the next finer scale model. Other choices are possible, fluxes or a combination of fluxes and values, but the value (or Dirichlet) condition is considered to be best suited for the present modelling task. Some further views on this problem will be given in the Discussion section.

Another problem with the embedded grid technique concerns the fracture network. In the author's view, it is essential to realise that mid-sized fractures (which may not belong to the identified deterministic fractures) may control the

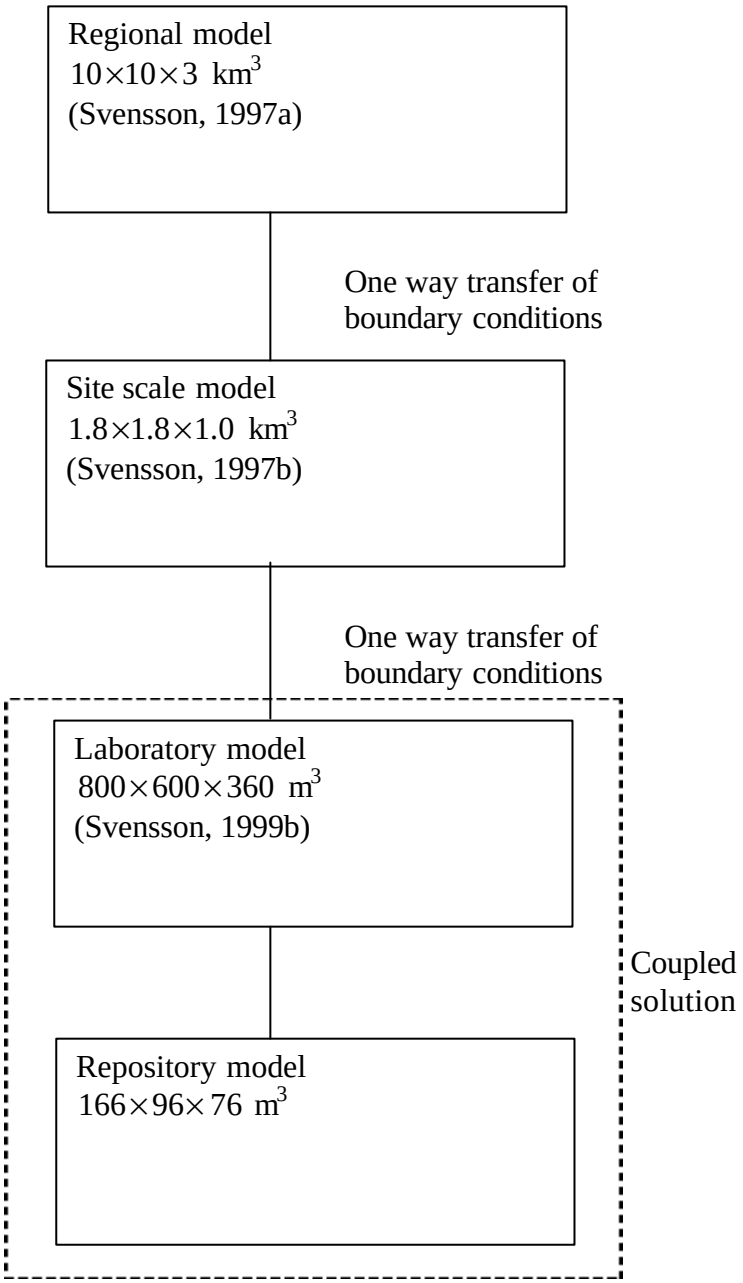

Figure 2-1. *The range of model scales considered when deriving boundary conditions for the present modelling task.*

pressure in the embedded grid completely. In Figure 2-2, illustrations of some possible situations are shown. Let's assume that the large fracture zones control the pressure distribution generally, giving a mean gradient in the "up-down direction". Next consider some mid-sized fractures that are in contact with the major zones at one end. As there will be now flow in these fractures a uniform pressure, set by contact with the major zone, will prevail in the fracture. In Figure 2-2 a smaller area, indicating an embedded grid volume, is also shown. It is clear from the figure that the mid-sized fractures may control the mean pressure gradient in the embedded grid volume completely. By similar arguments one can expect that also the next size-class of fractures, perhaps comparable to the length scale of the embedded grid, are important for the pressure in, and at the boundaries of, the embedded grid.

Ideally the same fracture network should be used for both grids. This may however not be feasible as the embedded grid volume may require a smaller minimum fracture size, as high resolution is the purpose of the embedded grid, and this fracture size may generate more fractures in the large grid than can be handled computationally.

These observations about the fracture network resulted in the following approach:

- Mid-sized fractures. A large number of realisations are tested and a set of criteria are used to sort out acceptable realisations. If, as an example, a mid-sized fracture (say a length scale larger than 100 m) is present close to the Repository this realisation is rejected as all large fractures close to the Repository are assumed to have been identified. The set of criteria used will be further discussed in the Calibration section.

- Coarse grid (Laboratory model). Fractures down to a size of 5 metres, which is equal to the cell size used, are generated.

- Embedded grid (Repository model). All fractures from the coarse grid domain that are in, or in contact with, the embedded domain are imported to the embedded grid. Fractures larger than 50 metres and close to the Repository (details in next section) are however removed as all large fractures close to the Repository are assumed to be known and are hence to be treated as deterministic features. Fractures in the range 1-5 metres, the cell size in the embedded grids is 1 metre, are then generated stochastically and combined with the deterministic fractures in the domain and the fractures from the coarse grid, which are also treated as deterministic in the embedded grid.

2.3 OBJECTIVES OF CALIBRATION

In the approach outlined certain realisations are to be rejected. If we allow ourselves to pick realisations that meet some criteria, one can not claim that the chosen realisations follow the basic statistical distributions used; we may have chosen all realisations at one extreme end of the distribution. It is also the intention to remove large generated fractures in the embedded domain and replace these with identified, from field measurements, features of the same size class. Once again we may violate the basic statistical distributions.

These operations are however considered to be acceptable by noting that the objective of the study is to "provide realistic distributions of flow, pressure and salinity in the Prototype Repository area". The purpose is thus not to demonstrate

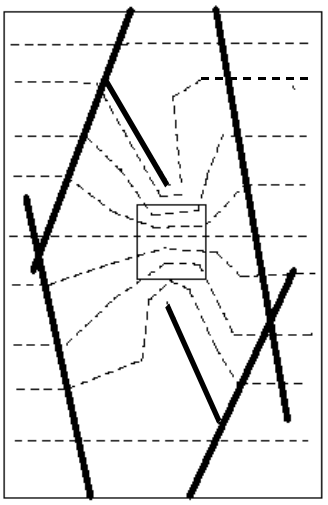

Extrem pressure
gradient in up-down direction
in embedded grid

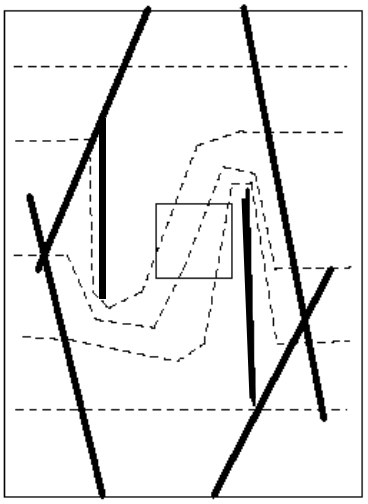

Extrem pressure gradient
in left-right direction in
embedded grid

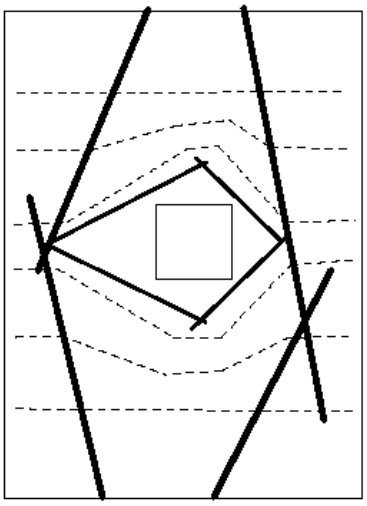

Zero pressure gradient
in embedded grid

Figure 2-2. *Illustration of how mid-sized fractures may determine the pressure conditions in an embedded domain.*

that the fracture networks represent conditions at the Äspö HRL generally. In the calibration process it will hence be comparisons with local field data that are in focus and the quality of the different realisations will be judged by the agreement with measurements. One way to characterise this approach is to say that “the general fracture network is conditioned, using data from the Repository area”.

2.4 CONCLUDING REMARKS

In the rest of the report the conditions around the Repository, and hence the Repository model, will be in focus. The Laboratory model is however an important part of the coupled system. The reason why the Laboratory model is not discussed in the Calibration section, and no results are shown in the Main result section, is that it has been verified previously, see Svensson (1999b). Some minor changes are introduced, but it will be assumed that the earlier calibration study is still valid.

3 MATHEMATICAL MODEL

3.1 BASIC APPROACH AND REQUIREMENTS

The Repository model will be used to characterise, in as much detail as possible, the conditions in the rock volume surrounding the Prototype Repository. The main variables of interest are: flow, pressure, salinity and hydraulic conductivity. With this in mind the following basic requirements of the simulation model have been formulated.

- It needs to be three-dimensional with as high resolution in space as possible. Both the fracture network and the various tunnels in the Repository area will be better represented in a grid with high resolution.
- Variable density needs to be accounted for as the salinity of the groundwater will vary in the domain.

The main computational domains were introduced in Figure 1-1. The motives for the size and orientation of the domains can be summarised as follows:

- The orientation should follow the Äspö coordinate system, to facilitate integration with the Äspö data base.
- The computational grid for the Laboratory model should preferably have a grid spacing of about 5 metres, in order to resolve the fractures and the fracture zones. For the domain indicated in Figure 1-1, this results in a grid of more than 1 000 000 cells. The grid size in the Repository model should be around 1 metre, to be able to resolve the details around the deposition holes.

These considerations led to a domain of 800 x 600 x 360 m^3 for the Laboratory model, centred around the Äspö HRL, represented in a computational grid of 160 x 120 x 72 cells (and hence a grid size of 5 metres). The size of the Repository model is 166 x 96 x 76 m^3, which with a grid size of 1 metre gives 1 211 136 cells. The coordinates (in the Äspö coordinate system) for the bottom south-west corners are: 1640 (x), 7000 (y), - 560 (z) for the Laboratory model and 1811.5 (x), 7221.5 (y), -488.0 (z) for the Repository model.

3.2 GOVERNING EQUATIONS

For the momentum balance it will be assumed that the Darcy law applies. For the salinity equation we will assume a balance between advective transport and diffusion, i.e. only steady state conditions are to be simulated. For the domain considered it can be expected that the strong forcing of the tunnel, i.e. the inflows, ensures more or less steady state conditions.

Within these assumptions, and the requirements listed in the previous section, the following set of equations can be formulated.

Momentum:

$$0 = -\frac{\partial p}{\partial x} - \frac{\rho g}{} \tag{3-1}$$

$$0 = -\frac{\partial p}{\partial y} - \frac{\rho g}{K_y} v \tag{3-2}$$

$$0 = -\frac{\partial p}{\partial z} - \frac{\rho g}{K_z} w - \rho g \tag{3-3}$$

Salinity balance:

$$\frac{\partial}{\partial x} us + \frac{\partial}{\partial y} vs + \frac{\partial}{\partial z} ws = \frac{\partial}{\partial x}\left(Dn \frac{\partial s}{\partial x} \right) + \frac{\partial}{\partial y}\left(Dn \frac{\partial s}{\partial y} \right) + \frac{\partial}{\partial z}\left(Dn \frac{\partial s}{\partial z} \right) \tag{3-4}$$

Mass balance:

$$\frac{\partial}{\partial x} \rho u + \frac{\partial}{\partial y} \rho v + \frac{\partial}{\partial z} \rho w = 0 \tag{3-5}$$

Equation of state:

$$\rho = \rho_0 (1 + \alpha s) \tag{3-6}$$

Where u, v, w are Darcy velocities, p pressure, s salinity (in %, by weight), K_x, K_y, K_z conductivities, D dispersion coefficient, n kinematic porosity, α a coefficient $\left(= 7.8 \times 10^{-3}\right)$, ρ_0 a reference density of water (= 1 000 kg/m^3), ρ density of water and g gravitational acceleration. The coordinate system is denoted x, y, z with x in the east direction, y north and z vertical upwards.

In the present analysis dispersion is assumed to be due to different flow paths and molecular exchange with stagnant parts of the fracture network, see Svensson (2001a) for a full discussion of these concepts. The dispersion coefficient in Equation 3-4 is hence representing molecular diffusion only. Dispersion due to exchange with storage volumes is considered to be a major contribution to the total dispersion effect (Svensson 2001, work in progress). This process is however not active for a steady state situation, as the exchange with storage volumes is then zero.

3.3 GEOMETRIC FRAMEWORK AND MATERIAL PROPERTIES

The major transmissive fracture zones in the region are shown in Figure 3-1. Their transmissivities have been estimated by Rhén et al. (1997) and later somewhat modified in a calibration presented in Svensson (1997b). In Table 3-1 the transmissivities of the fracture zones considered in the present computational domains, see Figure 1-1, are given. The calibrated values will be used in this study. Also the thicknesses of the fracture zones (from Rhén et al., 1997) are given in Table 3-1. In the following we will call these major fracture zones the deterministic fracture zones in contrast to the background, or stochastic, fracture network to be described next.

Fracture properties. The relations used to determine fracture properties, like transmissivity and porosity, are taken from a recent evaluation/ compilation (Svensson 2001, work in progress). This compilation is far from exhaustive or complete, but is what is presently available. The following summarises the main relations:

- Transmissivity-fracture size:

$$T = \begin{cases} 10^{-5}(l/100)^2 \ \ [m^2/s] \text{ for } l \le 100 \text{ metres} \\ 10^{-5} \qquad\quad [m^2/s] \text{ for } l > 100 \text{ metres} \end{cases} \tag{3-7}$$

  where T is transmissivity and l fracture size.

- Transmissivity-transport aperture: Based on empirical relations and the cubic law it was found that the transport aperture, e_T, can be estimated as:

$$e_T = 2.0T^{0.6} \tag{3-8}$$

- Fracture size-thickness: Field data from Äspö HRL indicate that a fracture thickness, b, of 1% of the fracture length is a good choice. The fracture thickness is defined to include the flow channel, the gauge material, parallel flow paths, etc. It is hence often one or two orders of magnitude larger than the aperture. The kinematic porosity, n, is calculated from e_T and b ($n = e_T / b$).

- Diffusion coefficients: Molecular diffusion in a conductive element should be proportional to the product of the transport porosity and the diffusivity value in the pore water (Neretnieks, 1993). The proportionality constant is related to the properties of the pore space (constrictivity and tortuosity). In the simulations carried out in this report, we will simply assume that the diffusion coefficient for a conductive element is equal to the product of the kinematic porosity and the diffusion value in pure water (= 10^{-9} m^2/s).

Fracture orientation. Several projects have been carried out with the objective to characterise the fracture orientation at Äspö. Of special significance for this study are: the TRUE Block Scale Volume the ZEDEX tunnel

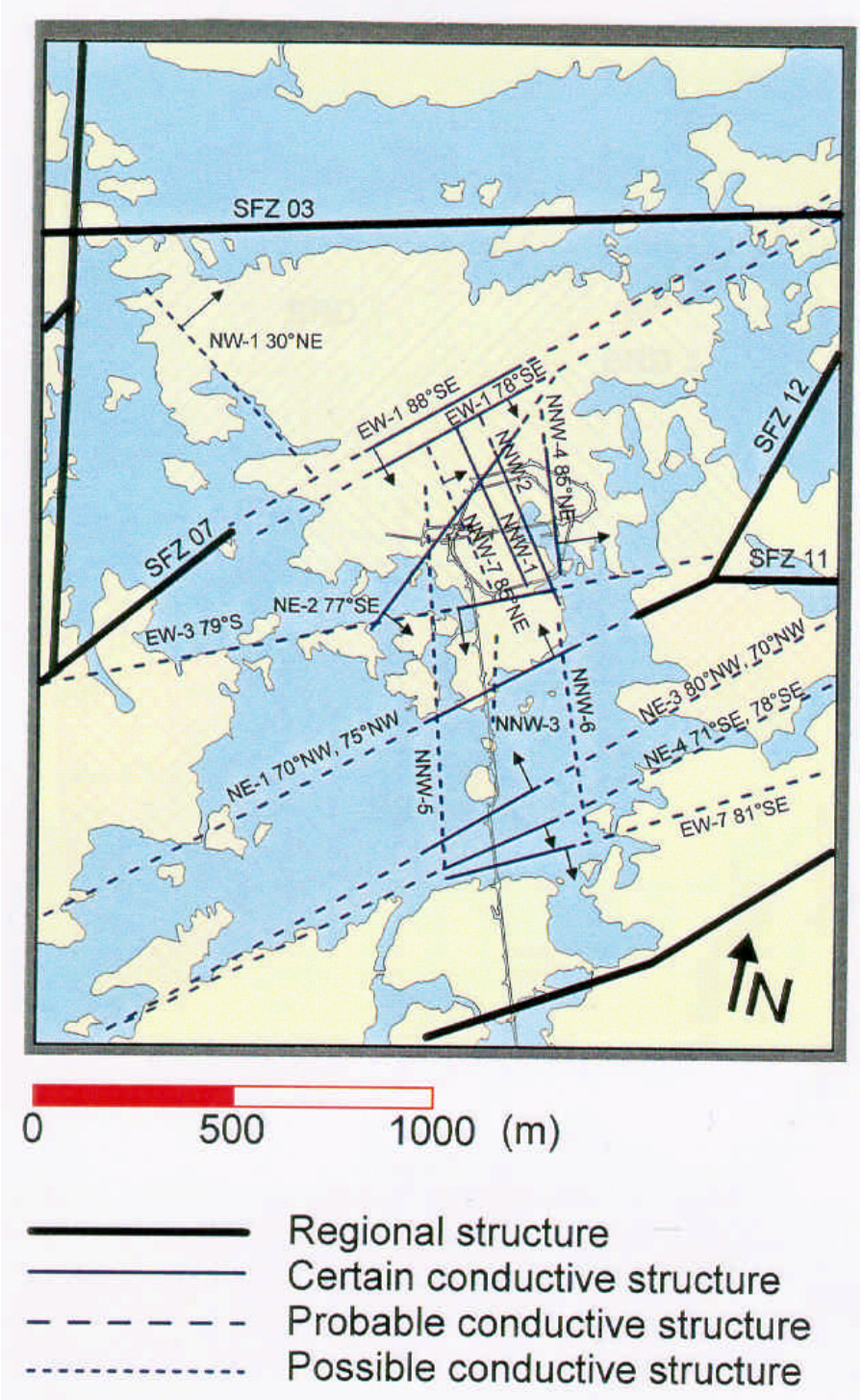

Figure 3-1. *Major fracture zones in the area, after Rhén et al. (1997).*

(Hermansson et al., 1998) and the TBM tunnel (LaPointe et al., 1995). These rock volumes are part of the present domain and we therefore seek a consensus based on the above mentioned reports. The following is suggested:

> Three major fracture sets can be identified; one horizontal, one NW trending and one NE trending. The two last ones are subvertical. The horizontal fracture set is believed to be less water conducting. The NW trending set is more conductive, or of higher intensity, than the NE trending set.

From this it is concluded that the fracture network can be based on two vertical fracture sets; one NE trending and one NW trending. Furthermore, in the above mentioned reports the spread around these main orientations was given in form of a Fisher dispersion coefficient, κ. Also in this study we will use a Fisher distribution for the realisation of the network. As the NW-direction should be more conductive, 70% of the fractures will have this trend (with Fisher's $\kappa = 12$) and 30% will have a NE trend (with $\kappa = 7$). This specification was obtained from the calibration of the Laboratory model (Svensson, 1999b) and also seems to be in fair agreement with the recent compilation of data by Stigsson et al. (2000).

Fracture intensity. The fracture intensity is specified from a power law distribution. For a length interval, *dl*, we then get:

$$n = \mathrm{I} * \left[\left(\frac{l + dl}{l_{ref}} \right)^{\alpha} - \left(\frac{l}{l_{ref}} \right)^{\alpha} \right] / \alpha \qquad (3\text{-}9)$$

where n is the number of fractures per unit volume, I the intensity, l_{ref} a reference length (=500 m) and α, the power law exponent, put to -2.6 (see LaPointe et al., 1999). The intensity was determined to 10^{-8} by generating fractures in the interval 320 to 1 000 metres and compare the number with the number of deterministic fracture zones in the Laboratory domain. The intensity chosen gives 10 to 15 (different realisations) fracture zones in the length interval which can be compared to 12 deterministic fracture zones.

Fracture shape: The fractures are assumed to be squares, with length, *L,* and have a constant thickness, *b*. In Rhén et al. (1997) major fracture zones are said to have a thickness larger than 5 metres. The thickness of the deterministic fracture zones are given in Table 3.1 and, as can be seen, all fracture zones have $b \geq 10$ metres. The background fractures have a thickness, *b*, equal to 1% of the fracture length.

From this information the background fracture network for the Laboratory model, specified in Table 3-2, can be formulated. As seen, fractures from 5 to 320 metres are generated. The lower limit was chosen to be the same as the grid resolution as only fractures larger than the grid size can contribute to the anisotropy and correlation in the conductivity field. The upper limit is chosen with respect to the deterministic fracture zones, which are typically larger than 300 metres.

For the Repository model fractures larger than 5 metres are imported from the Laboratory model. Fractures in the size class 1-5 metres are generated stochastically; Table 3-3 summarises the properties of these fractures.

Deterministic features in Repository area. As mentioned some major conductive features in the vicinity of the Repository have been identified (Forsmark and Rhén, 1999). Two of these, North Major Feature and South Major Feature, are included in the Repository model, both with a transmissivity of 8×10^{-8} m^2/s. The locations of these features are given in Figure 3-2. Also some fractures from the TRUE Block Scale experiment are included as deterministic features. Based on an evaluation by Rhén (2001) (Pers. comm.), features 6, 7, 13, 19 and 20 with properties given in Hermansson and Doe (2000) were included. The positions of these fractures are given in Figure 3-2.

3.4 SPATIAL ASSIGNMENT METHOD

All fractures (deterministic and background) will be represented in the computational grid by the method described in Svensson (1999a). However, before the fractures are represented as grid conductivities, diffusivities and porosities, one needs to consider how isolated fractures are to be treated. Depending on the situation studied we may choose to remove or keep isolated fractures, or groups of fractures. In the simulations of the Laboratory volume, we choose to remove the isolated fractures and the following steps are then performed:

- The deterministic fractures are considered to be water-conducting and can thus form a "starting" network in the sorting procedure.
- Fractures that cross the boundaries of the domain are not removed as we can not for certain say that these are isolated.
- A sorting procedure determines if a fracture, or a group of fractures, is isolated and, if so, removes these fractures.

However when fractures are exported to the Repository volume we choose to keep all fractures, as we can not for certain say that these fractures will be isolated when fractures in the size class 1-5 metres are added.

Finally a small background conductivity will be added to all cells, both in the Laboratory and Repository models. This conductivity will be further discussed in the Calibration section.

3.5 BOUNDARY CONDITIONS

For the cases considered in this report the boundary condition are given as prescribed pressure and salinity. These are generated from the Site scale model. Since the grid size in the Site scale model is 20 metres, and 5 metres in the Laboratory model, linear interpolation was used to generate the intermediate values.

As the Äspö HRL is included in all simulations, we need to consider the inflows to the tunnel. These inflows are not boundary conditions in the usual meaning; a more relevant name is perhaps "distribution mass sinks". The measured inflows to tunnel sections need to be assigned to computational cells with a deterministic fracture zone crossing. Based on the measured data given by Rhén et al. (1997),

Table 3-1. Properties of the deterministic fracture zones.

Fracture zone	Thickness (m)	Transmissivity (m^2/s) x 10^{-6}	Transport aperture (m) x 10^{-3}	Kinematic porosity x 10^{-3}
EW1, 88º	20	0.52	0.34	0.017
EW1, 78º	20	12.0	2.23	0.11
EW3	10	12.0	2.23	0.22
NE2	10	8.0	1.75	0.175
NE1a	10	150.0	10.16	1.02
NE1b	10	150.0	10.16	1.02
NNW1	10	30.0	3.87	0.39
NNW2	10	10.0	2.00	0.20
NNW3	10	20.0	3.03	0.30
NNW4	10	65.0	6.15	0.62
NNW5	10	4.0	1.15	0.12
NNW6	10	14.0	2.45	0.25
NNW7	10	80.0	6.96	0.70
NW1	10	0.41	0.29	0.03

Table 3-2. Properties of the fractures forming the background fracture network for the Laboratory model. Thicknesses, apertures and porosities are constant within each length interval and calculated from an average length in the interval.

Fracture set	Length interval (m)	Thickness (m)	Number of fractures generated	Number of fractures isolated	Trans-missivity (m^2/s) x 10^{-6}	Transport aperture (m) x 10^{-3}	Kinematic porosity x 10^{-3}
1	160-320	2.08	28	0	10.0	2.0	0.96
2	80-160	1.04	120	0	10.0	2.0	1.92
3	40-80	0.52	514	9	2.7	0.91	1.75
4	20-40	0.26	2707	408	0.68	0.40	1.53
5	10-20	0.13	15563	5343	0.17	0.17	1.33
6	5-10	0.05	91336	48434	0.04	0.07	1.46

Table 3-3. Properties of the fractures forming the background fracture network for the Repository model. Thicknesses, apertures and porosities are constant within each length interval and calculated from an average length in the interval.

Fracture set	Length interval (m)	Thickness (m)	Number of fractures generated	Number of fractures isolated	Trans-missivity (m^2/s) x 10^{-8}	Transport aperture (m) x 10^{-3}	Kinematic porosity x 10^{-3}
1	2.5-5.0	0.03	4200	2200	0.90	0.03	1.00
2	1.0-2.5	0.013	45800	34600	0.16	0.01	0.77

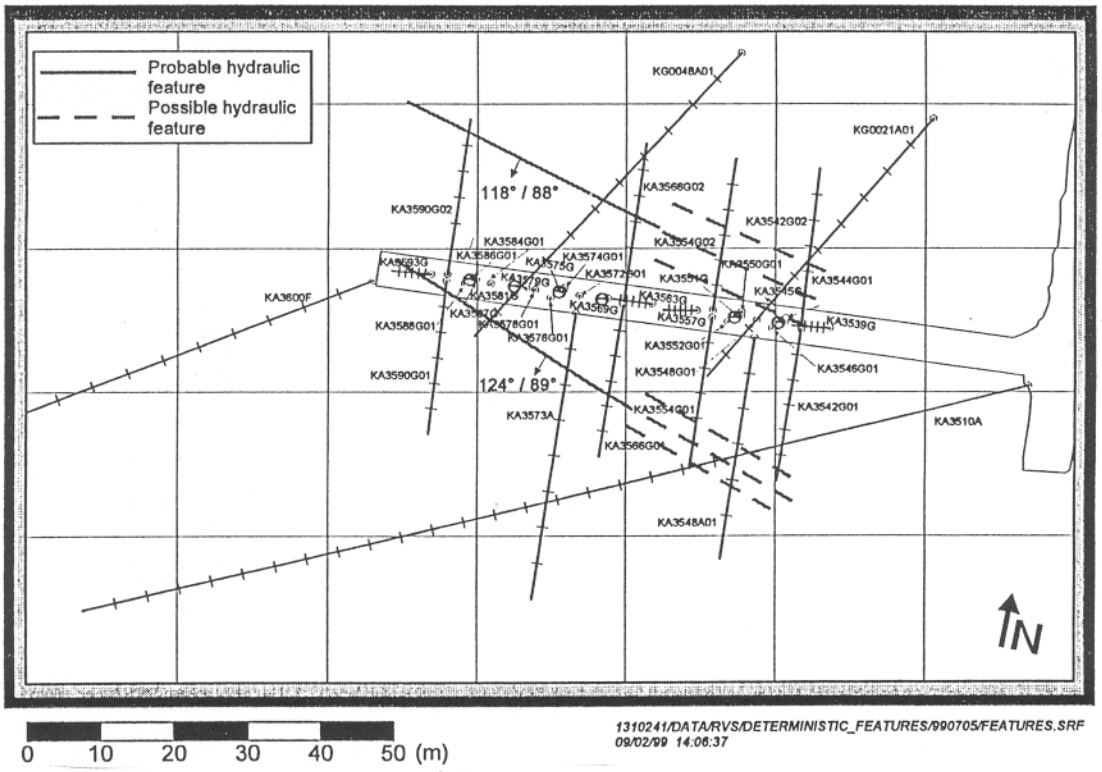

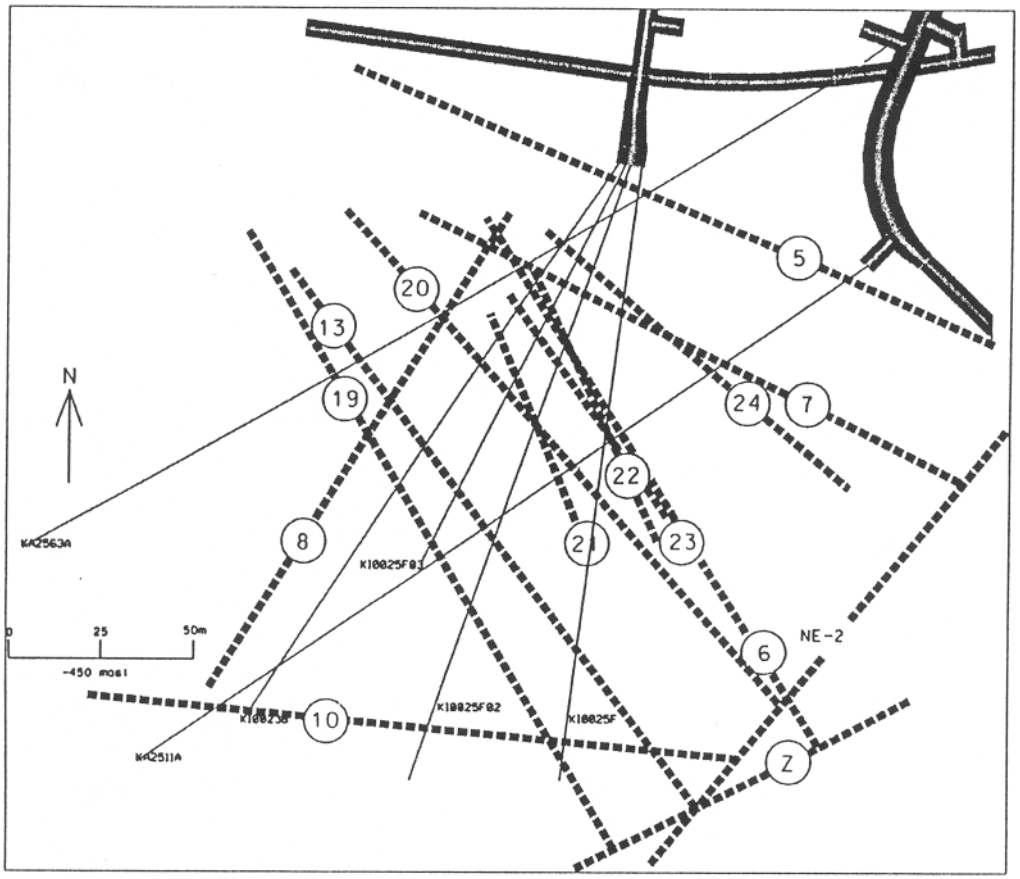

Figure 3-2. *Local deterministic features around the Repository (top) and in the TRUE Block Scale area (from Hermansson and Doe, 2000).*

the distribution found in Table 3-4 have been estimated. This method is used for the Laboratory model.

An alternative way to describe the influence of the tunnel is to apply a fixed pressure, i.e. atmospheric pressure, in the "tunnel cells". Normally a larger inflow than measured will then result and it will be necessary to reduce the conductivity of the cells facing the tunnel. The strength of this extra friction, or skin-resistance, can be determined in an iterative manner from the measured inflow to a certain tunnel section. This method is to be preferred, if the pressure distribution close to the tunnels is of interest and will be used for the Repository model.

For the second alternative to handle the tunnel inflows, the tunnel geometry needs to be specified. This is done by determining if a cell centre is located in a tunnel or in the rock, using a CAD model of the tunnel. Some details of this method are given in Appendix B. Tunnel cells were then given an atmospheric pressure, while a cell with at least one cell wall facing the tunnel, has a skin applied to all cell walls.

3.6 NUMERICAL TOOL AND OUTPUT PARAMETERS

The system of equations is solved by a currently developed code, called DarcyTools. The first version of DarcyTools will be presented in Svensson (2002, work in progress). Output parameters from the code are pressure, concentrations and Darcy velocities. It is however simple to generate additional output parameters like hydraulic head or particle tracks.

Table 3-4. Inflows to the Äspö HRL. Measured inflows and assigned fracture zones for withdrawal. Basic data from Rhén et al. (1997).

Tunnel section (m)	Measured inflow l/s	Selected zone(s) for withdrawal
1460-1584	0.61	NE2
1584-1745	0.27	NNW7
1745-1883	0.36	NNW1, NNW2
1883-2028	0.47	NNW4
2028-2178	0.70	NNW4
2178-2357	1.42	NNW1, NNW2
2357-2496	0.17	NE2
2496-2699	0.93	NNW7
2699-2875	0.38	NNW1, NNW2
2875-2994	1.12	NNW4
2994-3179	2.33	NNW4
Shaft	1.54	NNW7

4 CALIBRATION

4.1 INTRODUCTION

As mentioned above, a new groundwater model (DarcyTools) will be used for the simulations. DarcyTools has so far not been rigorously tested and verified and is, strictly speaking, not ready for the present task. However, verification and validation studies are underway and most parts of DarcyTools have been tested and applied when the PHOENICS (Spalding, 1981) code was used as an equation solver. In DarcyTools a new solver, called MIGAL, is used and this is the main new component in DarcyTools. Some preliminary tests, intended to demonstrate that MIGAL solves the system of equations correctly, have been performed. The outcome of these tests can be found in Appendix A. These first tests show that MIGAL solves the basic equations correctly, but more work is of course needed, and will be reported, before one can claim that the accuracy of DarcyTools has been demonstrated.

The objective of the calibration process was discussed in Section 2. However, it may be in place to recall that we are interested in five realisations of the conductivity field that give accurate flow and pressure distributions in the Repository area. With accurate we mean that close agreement with field data can be demonstrated. The focus of the calibration will be on flow and pressure. Salinity data are available, but as the salinity is fairly uniform in the area it was concluded that it is not possible to discriminate between different realisations from this information.

4.2 CALIBRATION CRITERIA

With the objective in mind, it was concluded that the following criteria ought to constrain the model in a useful way:

- Tunnel inflows. Measurements and estimates of the inflow to different tunnel parts are available, see Forsmark and Rhén (1999) and Stigsson et al. (2000). A recent re-evaluation (Rhén, 2001, Pers.comm.) of the inflow data has however revealed that the inflows are 2-3 times higher than given in the reports mentioned. Based on this information, the inflow to the tunnels has been divided into three parts, see Figure 4-1. The model should predict these inflows as closely as possible.

- Borehole pressures. Extensive data on borehole pressures, before, under and after the excavation of the deposition holes, are available, see Forsmark and Rhén (1999), Forsmark et al. (2001). The pressure measurements before the excavation will be compared with calculated pressures. Also the relation “Pressure-Distance from tunnel” will be studied as this is considered to be a well established relation from field data.

- Conductivity statistics. The conductivity distribution for the 1 metre scale has been estimated from borehole sections. This distribution will be compared with the cell conductivities in the Repository model (which has a cell size of 1 metre). It is however not obvious that field data from a packer spacing of 1 metre can be directly compared to the grid conductivities.

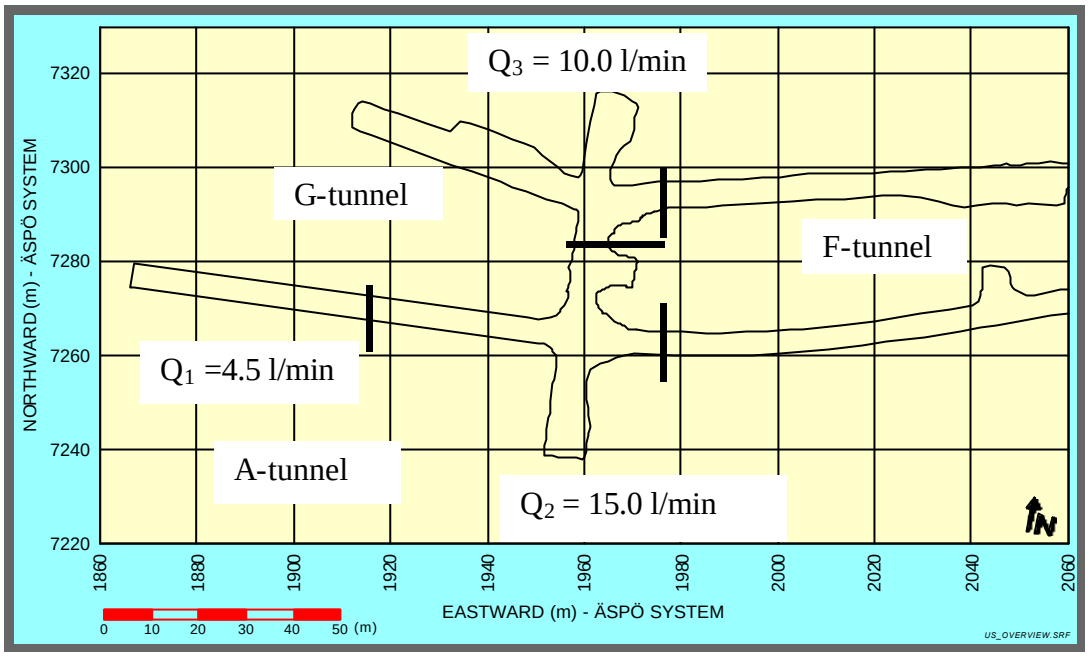

Figure 4-1. *Total inflow to the tunnels is partitioned into three inflows.*

4.3 CALIBRATION PROCESS

The methods and concepts, embedded in DarcyTools, have earlier been applied to larger scale problems, i.e. the Laboratory and Site scale models. The pressure distribution around a tunnel is quite a different problem and it was not clear if, for example, the type of fracture network generated would be suitable also for this problem. However, it was decided to follow the procedures from the Laboratory model as a first test. Fracture properties, orientation, intensity, etc were thus determined from the formulae given in Section 3, also for the Repository model. In the Laboratory model a background conductivity with a lognormal distribution was used as a tuning knob; the same approach will be used for the Repository model.

Preliminary tests showed that it ought to be possible to generate five realisations that fulfilled the criteria, simply by tuning the background conductivity. The following steps can thus describe the calibration process:

- Generate a large number of realisations of the conductivity field and select the five best based on the following criteria:
  - No large fracture, with its centre outside the Repository model, should be present close to the tunnels (Note that large fracture with centres inside the domain have been removed).
  - A "realistic" inflow (say 10 – 50 l/min, without skin) in each tunnel section shown in Figure 4-1. If a large fracture crossed a tunnel an inflow of perhaps several hundred l/min was generated, which means that the two conditions are partly linked. However, also a zero inflow case (or close to zero) has to be rejected, due to the first calibration criterion chosen.
- For the five realisations chosen, verify that the application of a skin around the tunnels can force the inflows to the desired values.
- Adjust the mean of the background conductivity, K_0, to get good agreement with the pressure data from boreholes. The standard deviation $(\text{for } \log_{10} K_0)$ of the added conductivity was fixed to 1.0.
- Check that the conductivity statistics for the 1 metre scale is in fair agreement with field data.

4.4 RESULTS

Twenty realisations of the conductivity field were generated in order to select five acceptable. Some of these twenty realisations generated an inflow of several hundred l/min, others zero, in a tunnel section.

The five best could however be forced, by way of a skin factor, to give a correct inflow for all three tunnel sections shown in Figure 4-1. The skin factor multiplied all cell wall conductivities of the cells facing the tunnel. As can be seen in Table 4-1 the skin factors are in the range 0.02 – 10. The upper limit for the skin factor was set to 10.0 and, as can be seen, this skin was applied for Q_2 in realisation 3. The inflow is still a little bit lower than desired.

In Table 4-1 also the mean values for the added background conductivity are given; these are in the range 3.0 – 6.5 x 10^{-10} m/s. The values were determined

from a comparison with measured pressures in borehole sections, see Table 4-2. In this comparison we will intentionally call the difference between the measured and calculated pressures a “difference” and not an error, as an error is something that can be identified and corrected. Anyway, the objective of the calibration, using the added conductivity as a tuning knob, was to bring down the mean difference to a small value; as can be seen in Table 4-2 this was successful. If we like, one can consider the added conductivity as representing fractures smaller than the smallest fracture generated in the network, i.e. smaller than 1 metre. A conductivity value of around 10^{-10} m/s seems to be of the right magnitude to simulate such fractures. In Table 4-2 also the number of comparisons with an absolute difference in head, smaller than 100 metres is given; this gives an additional measure of the comparison. It should be added that more pressure recordings than given in Table 4-2 are available. The ones selected are those that were classified as “best quality” in Forsmark and Rhén (1999).

Another way of representing the comparison of pressures in Table 4-2, is shown in Figure 4-2. Now the pressures, measured and simulated, are shown as a function of the distance to the nearest tunnel centre. As we are interested in the nearfield around the tunnels, this way of plotting the information is of interest. The first diagram in Figure 4-2 shows the mean of all five realisations, as compared to the evaluated trend in the measured data. The trend in the measurements was estimated by fitting a straight line to the measured heads in Table 4-2. The rest of the diagrams show comparisons for each realisation. From Figure 4-2 one can conclude that the pressure head may vary with several hundred metres at a distance of, say, 10 metres from the tunnel centre. Further, the simulations show the same trend and spread as the measurements.

Finally, we will check the conductivity statistics. As mentioned above, it will be assumed that the 1 metre cell conductivities can be compared to the conductivities obtain from borehole measurements with a packer spacing of 1 metre. The distributions from the five realisations are given in Table 4-3 and in Figure 4-3 the mean of the five realisations is compared to the measured distribution. It is found that the agreement is good for conductivities above 10^{-9} m/s, while a deviation is found below this value. The distribution is however sensitive to the value of the added background conductivity for small conductivities. This is illustrated in Figure 4-3, where the distribution for a background conductivity of 10^{-11} m/s is also shown. As can be seen this will result in a perfect agreement with the measured distribution. It was however regarded as more important to optimise the agreement with the pressure measurements, and the background conductivities given in Table 4-1 are thus kept.

4.5 CONCLUDING REMARKS

It can be concluded that five realisations of the conductivity field, that fulfill the calibration criteria, have been found. The agreement with measurements is generally very good.

It is worth noting that this was achieved by adding a small background conductivity, while the basic methods and parameter estimates are kept from the Laboratory scale model.

Table 4-1. Inflows, skins and background conductivities for the Repository model. Skin factors are given with high accuracy in order to facilitate later comparisons.

Realisation	Q_1 l/min	Q_2 l/min	Q_3 l/min	$Skin_1$	$Skin_2$	$Skin_3$	Mean conductivity added m/s [x 10^{-10}]
1	4.5	15.0	10.0	0.0259	7.3655	0.1019	3.0
2	4.5	15.0	10.0	0.0715	0.0995	6.1238	5.0
3	4.5	13.6	10.0	0.0255	10.000	0.2430	6.5
4	4.5	15.0	10.0	0.0713	0.2595	0.0793	6.5
5	4.5	15.0	10.0	0.4360	0.0608	0.0352	3.0

Table 4-2. Comparison between measured pressures in borehole sections and simulated pressures from five realisations of the fracture network.

Borehole	Measured Head [m]	Realisation									
		1		2		3		4		5	
		Head	Diff.	Head	Diff.	Head	Diff.	Head	Diff.	Head	Diff.
KA3510A:3	393.2	404.3	11.1	407.4	14.2	394.6	1.3	411.2	18.0	425.5	32.2
KA3539G:1	308.2	311.3	3.1	243.7	-64.5	289.9	-18.3	291.9	-16.3	338.4	30.0
KA3542G01:1	378.7	364.5	-14.1	323.3	-55.2	304.4	-74.1	319.6	-58.9	389.8	11.4
KA3542G02:1	321.9	154.2	-167.7	240.6	-81.3	134.1	-187.8	202.6	-119.3	235.1	-86.8
KA3550G01:1	18.1	220.5	202.4	256.7	238.5	174.4	156.2	198.6	180.5	230.5	212.4
KA3550G02:1	377.6	382.1	4.5	378.8	1.2	358.9	-18.7	376.9	-0.7	405.8	28.2
KA3563G01:1	327.8	261.8	-66.0	288.2	-39.6	269.1	-58.7	269.6	-58.2	302.8	-25.0
KA3563G01:2	142.0	389.7	247.6	347.3	205.2	336.5	194.5	341.9	199.9	292.2	150.2
KA3563G01:3	142.1	187.8	45.7	218.9	76.8	206.3	-64.2	169.9	27.8	267.6	125.5
KA3566G02:1	24.6	188.5	163.9	201.6	177.0	176.8	152.2	138.1	113.4	219.2	194.6
KA3566G02:2	349.2	354.6	5.4	296.6	-52.6	333.6	-15.6	323.2	-26.0	337.6	-11.6
KA3572G01:1	353.6	298.9	-54.7	298.3	-55.3	308.9	-44.7	300.6	-53.0	304.1	-49.5
KA3573A:1	191.5	359.3	167.8	303.2	111.7	316.8	125.3	286.3	94.9	280.1	88.7
KA3573A:2	404.9	366.7	-38.2	382.7	-22.2	371.8	-33.0	373.0	-31.8	324.5	-80.4
KA3579G01:1	391.5	280.3	-111.1	315.0	-76.4	316.0	-75.5	277.3	-114.2	289.4	-102.1
KA3584G01:1	204.1	416.7	212.6	322.6	118.5	348.3	144.2	323.7	119.6	280.0	75.9
KA3590G01:1	11.5	325.8	314.3	241.0	229.5	325.2	313.7	268.8	257.3	218.6	207.1
KA3590G01:2	395.6	425.1	29.5	382.1	-13.6	396.1	0.5	379.2	-16.4	326.7	-68.9
KA3590G02:1	389.8	340.5	-49.3	272.9	-116.9	332.9	-56.9	283.8	-106.1	227.8	-162.0
KA3590G02:2	368.0	350.5	-17.6	351.4	-16.7	382.2	14.1	360.7	-7.4	332.8	-35.3
KA3590G02:3	363.4	352.2	-11.2	339.8	-23.6	374.4	11.0	349.5	-14.0	315.4	-48.0
KA3590G02:4	276.8	339.1	62.3	320.3	43.4	362.0	85.2	332.1	55.3	285.8	8.9
KA3590G02:4	100.1	311.3	211.2	239.3	139.2	317.1	217.1	270.1	170.0	65.5	-34.6
KA3593G01:2	216.1	311.7	95.6	232.1	16.0	339.3	123.2	257.9	41.8	137.4	-78.6
KA3600F:2	409.7	404.9	-4.8	276.1	-133.6	372.5	-37.2	364.3	-45.4	315.2	-94.5
KG0021A01:2	349.5	114.0	-235.6	249.2	-100.3	197.6	-152.0	234.7	-114.9	271.3	-78.3
KG0021A01:3	349.6	68.7	-280.9	268.6	-81.0	163.9	-185.6	218.4	-131.2	255.8	-93.8
KG0021A01:4	331.7	88.5	-243.2	239.1	-92.6	159.2	-172.5	225.8	-105.9	263.8	-67.9
KG0021A01:5	231.1	149.2	-81.9	188.7	-42.4	111.3	-119.8	204.4	-26.6	261.5	30.5
KG0048A01:1	386.2	267.7	-118.5	277.2	-109.0	314.4	-71.8	268.1	-118.1	241.5	-144.7
KG0048A01:2	364.0	246.2	-117.8	278.1	-85.9	289.7	-74.3	267.1	-96.9	212.3	-151.7
KG0048A01:3	370.7	206.2	-164.5	272.2	-98.5	295.6	-75.1	276.5	-94.2	269.3	-101.5
KG0048A01:4	294.0	234.4	-59.5	132.3	-161.7	283.0	-11.0	254.6	-39.4	315.9	22.0
Mean Diff		-2		- 5		4		-3		-9	
Numbers with | Diff | < 100		18		21		20		20		23	

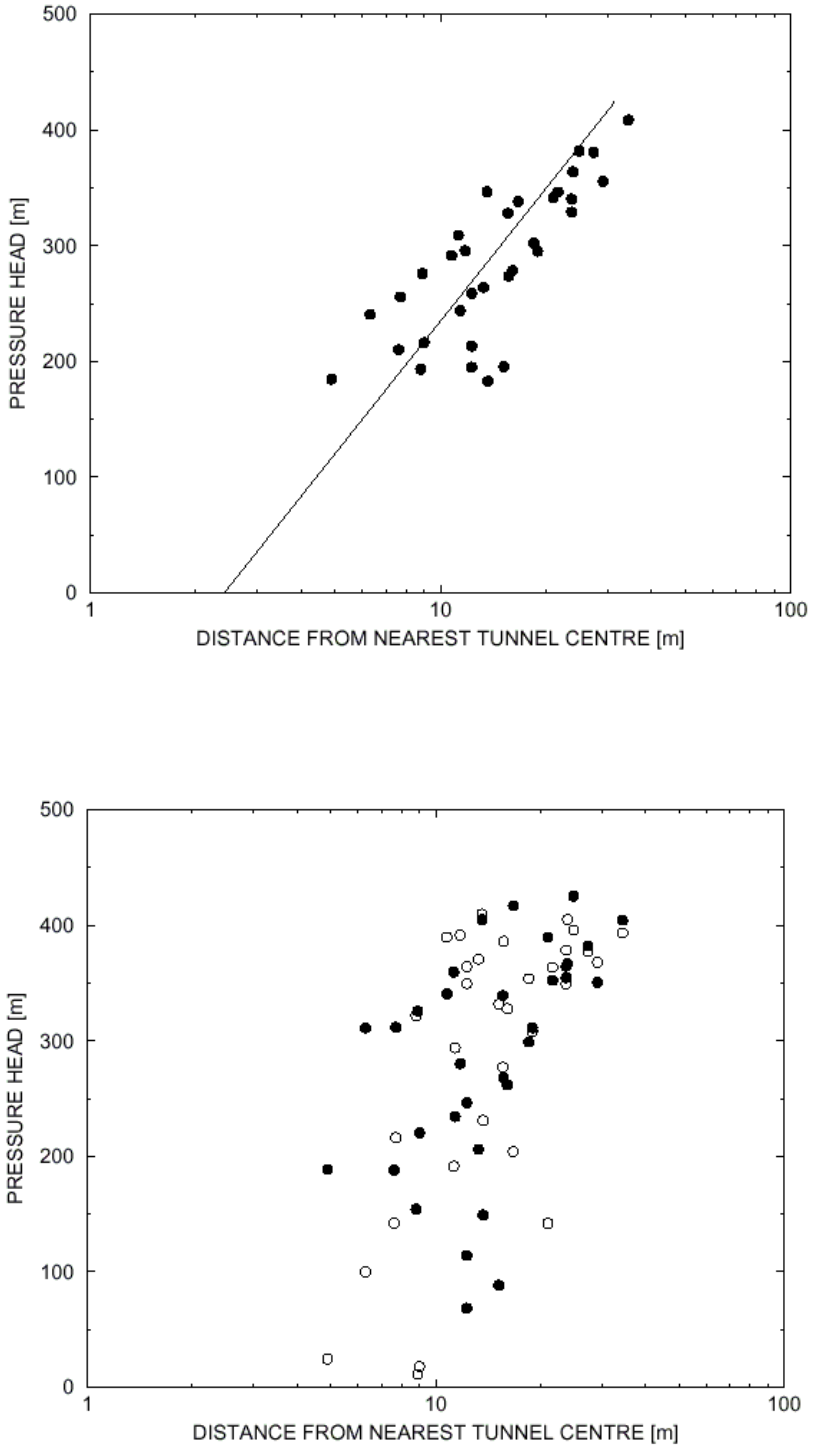

Figure 4-2. *Pressure head as a function of distance to nearest tunnel centre. Average of all five realisations compared to measured trend (top); straight line represents measurements.*
Bottom: Realisation 1 and measured data.
○ *Measurements*
● *Simulations*

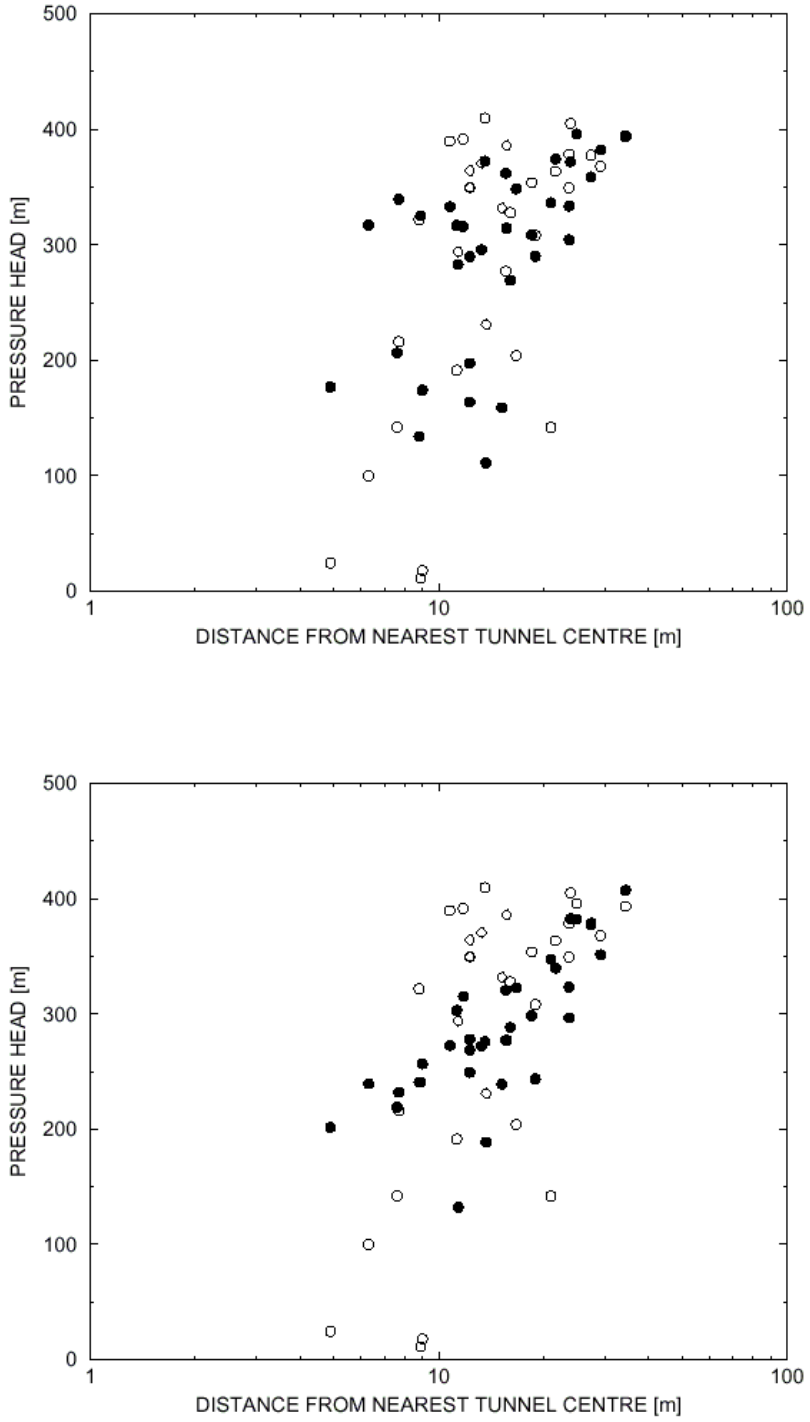

Figure 4-2, Cont. *Pressure head as a function of distance to nearest tunnel centre. Realisation 2 (top) and 3.*

○ *Measurements*
● *Simulations*

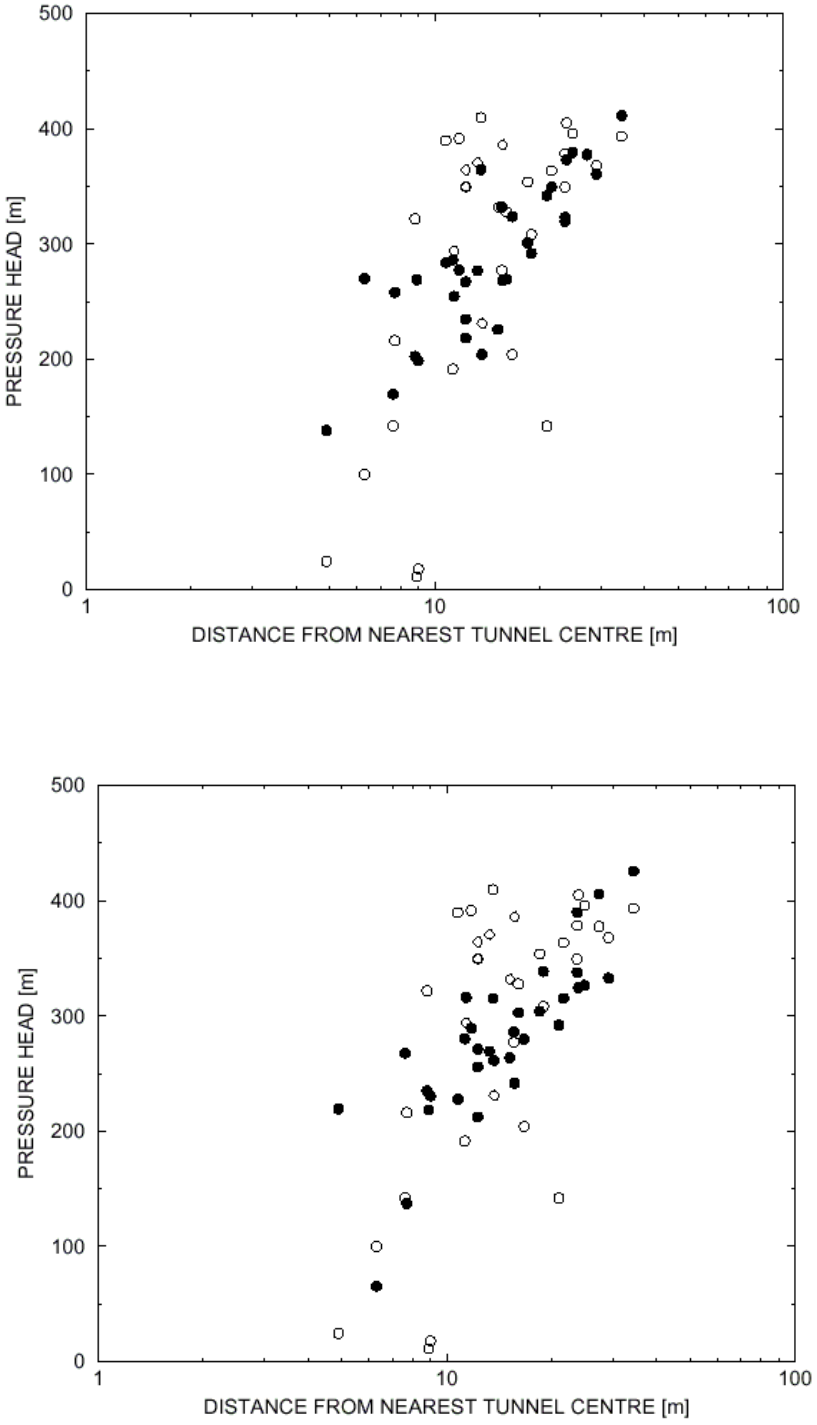

Figure 4-2, Cont. *Pressure head as a function of distance to nearest tunnel centre Realisation 4 (top) and 5.*
○ *Measurements*
● *Simulations*

Table 4-3. Simulated conductivity distributions. Five realisations and the average distribution.

Realisation	Cumulative conductivity distribution ($\log_{10}$ *K*, in %), *K* [m/s]						
	<-11	<-10	<-9	<-8	<-7	<-6	<-5
1	5	25	58	81	92	96	100
2	3	21	55	83	96	99	100
3	3	18	50	80	95	99	100
4	3	17	50	80	94	99	100
5	5	26	60	84	95	99	100
Average	4	21	55	82	94	99	100

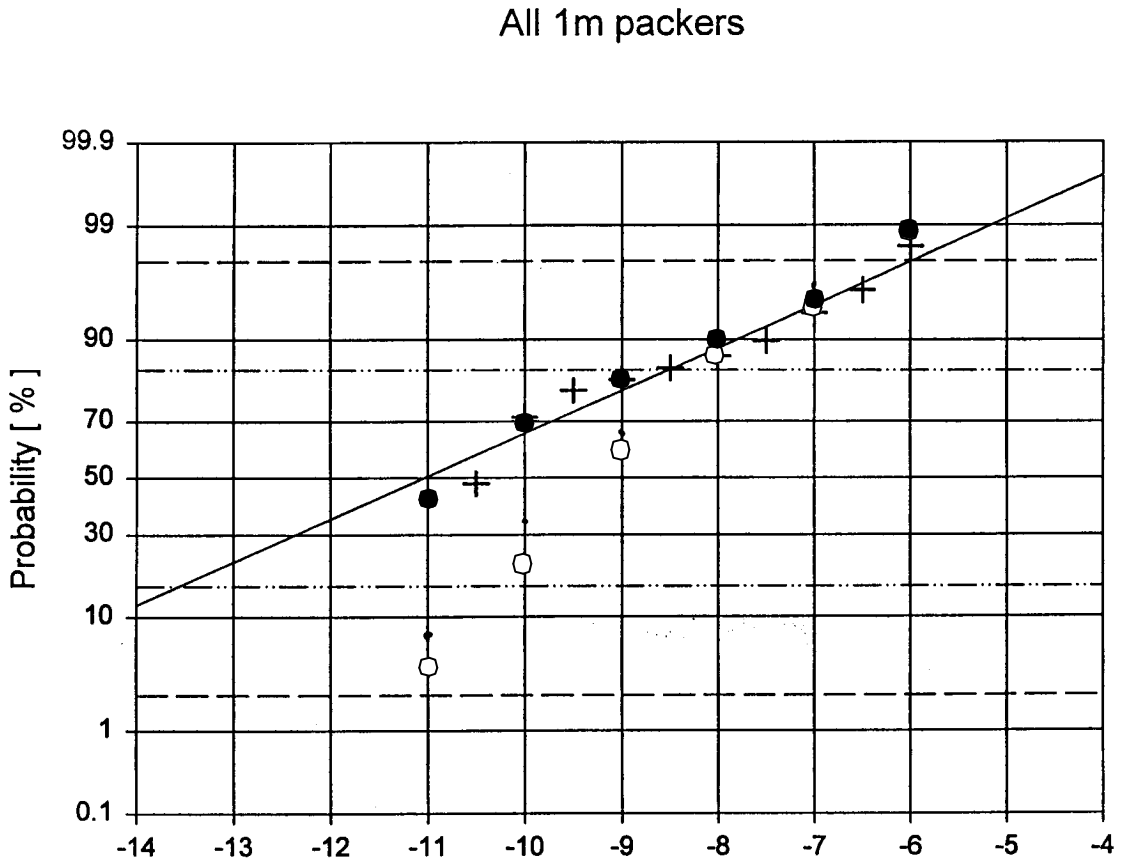

Figure 4-3. *Comparison between measured (line and crosses) and simulated conductivity distribution for a scale of 1 metre. (Basic figure from Stigsson et al., 2000).*

° Mean of five realisations
• Realisation 4 with an added conductivity of 10^{-11} m/s.

5 MAIN RESULTS

5.1 INTRODUCTION

With the calibrated model a number of steady state situations will be studied:

1. Atmospheric conditions in all tunnels and deposition holes.

2. Water saturated conditions in the inner and outer sections (to be defined) of the Prototype tunnel.
   a/ Skin for tunnels as in Case 1.
   b/ Skin for tunnels neglected.
   c/ For one realisation of the conductivity, use max and min values of the hydraulic conductivity of the backfill material. This for both case 2a and 2b.

These simulations will generate more data than can be easily described or illustrated. However, all results will be delivered as data files and all information can thus be retrieved and utilised. Information about available data files and formats is given in Appendix C.

The objective of the presentation of results given in this section is to illustrate the content of the data files and to provide a general, hopefully realistic, view of the flow, pressure and salinity distributions around the Repository.

Due to the many simulation cases it is not possible to show results for each realisation of the conductivity field. For some cases all five realisations will be given, for others only two. In these cases realisations 2 and 5 will be used. If only one realisation is used, it will always be realisation 5. There are no strong reasons for these choices; other realisations could have been used as well. It is however considered to be an advantage to always use the same two realisation, when two are to be used.

The hydraulic conductivity field will not be discussed or illustrated, even if it does control "much of the action". As a general background the conductivity fields for realisations 2 and 5 are therefore given in Figure 5-1. One can identify North and South Major structure close to the Prototype tunnel and also some deterministic features from the TRUE Block (in the lower part of the figure).

5.2 ATMOSPHERIC PRESSURE IN TUNNELS

In the calibration process, focus was on the pressure distribution for five realisation of the conductivity field. We will therefore choose to show horizontal sections, at the level –447 metres, of pressure for all five realisations. Also the salinity fields at this level will be shown, see Figures 5-2 to 5-6. It should be noted that the deposition holes are included in these simulations; the inflow to different sections (see Figure 4-1) is however kept, which means that the skin factors may be slightly modified, as compared to the calibration. The new skin factors are given in Table 5-1.

The main impression from the distributions given in Figures 5-2 to 5-6 is that the difference between different realisations is significant. In particular the salinity

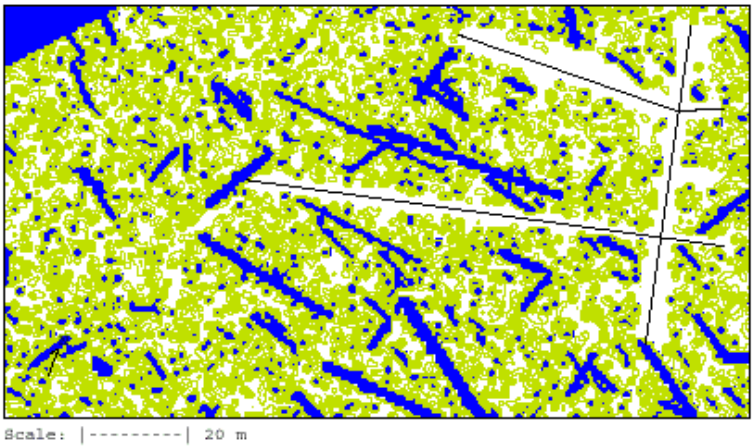

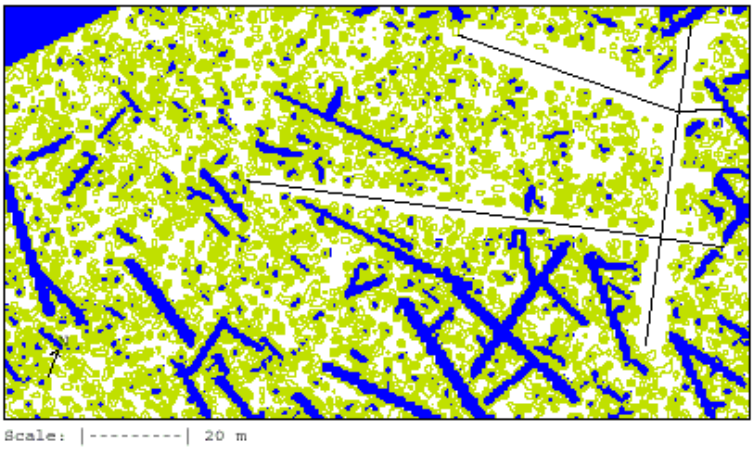

Figure 5-1. *Hydraulic conductivity fields for realisations 2 (top) and 5.*

Conductivity scale: $\begin{cases} \text{blue} > 10^{-8} \text{ m/s} \\ 10^{-9} < \text{green} < 10^{-8} \text{ m/s} \end{cases}$

field is highly irregular; a common feature is however that the salinity is higher south of the Repository, as compared to the area between the A and G tunnels. It is also possible to discern the influence of the skin factor in the pressure distributions. If the skin factor is small, i.e. a high reduction of the conductivity, the pressure gradient close to the tunnel will be large. This can be seen around the *G*-tunnel (see Figure 4-1) if realisations 2 and 5 are compared.

5.3 CLOSED A-TUNNEL

Next we will study what happens when the deposition holes and part of tunnel A are water saturated. The parts of tunnel A that are saturated are called section I and II and are defined in Figure 1-2. The buffer, which is used to fill the deposition holes, has a conductivity of 10^{-13} m/s. The tunnel sections are filled with backfill for which three (10^{-9}, 10^{-10} and 10^{-11} m/s) conductivities will be studied.

In Figures 5-7 to 5-10, some cases are shown in which the skin factors are varied (no skin or skin as for open tunnel). Realisations 2 and 5 are illustrated. It is found that the salinity and pressure distributions are not very sensitive to these changes.

Table 5-1. Skin factors with deposition holes included in the simulation.

Realisation	$Skin_1$	$Skin_2$	$Skin_3$
1	0.0253	5.8625	0.1022
2	0.0595	0.1063	9.9000
3	0.0227	10.000[1)]	0.2423
4	0.0616	0.2579	0.0797
5	0.1582	0.0606	0.0352

1) $_{2} = 13.9$ l/min

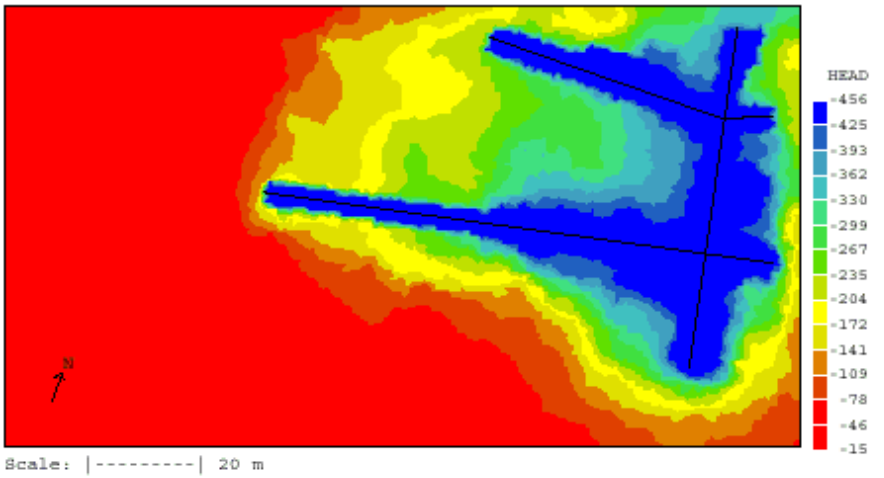

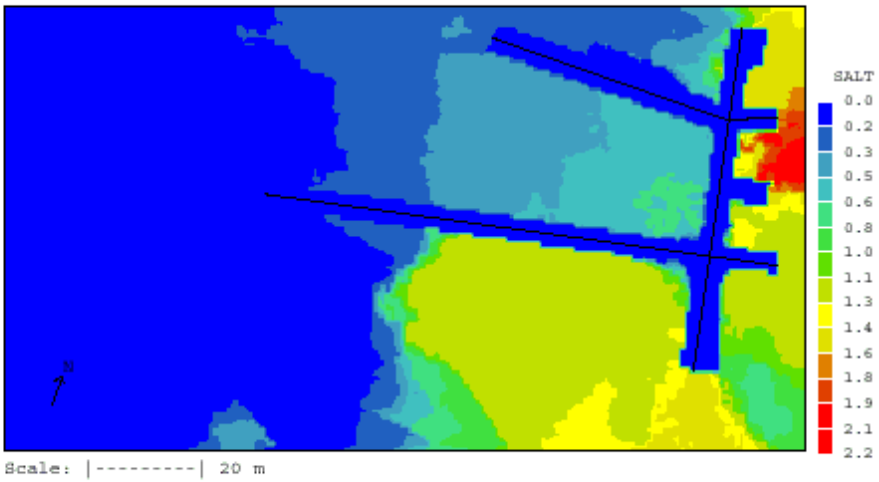

Figure 5-2. *Pressure head (in metres) (top) and salinity (in %) distributions at a depth of 447 metres below ground level.*
Realisation 1.

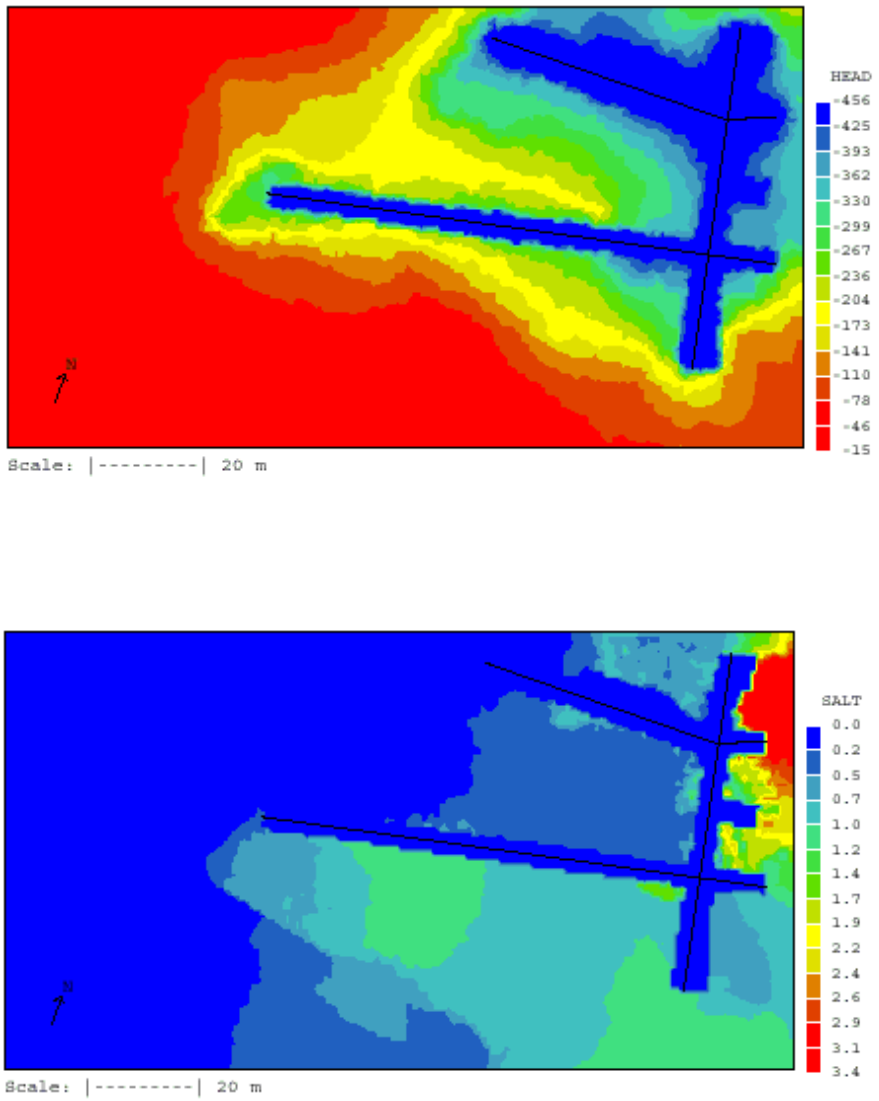

Figure 5-3. *Pressure head (in metres) (top) and salinity (in %) distributions at a depth of 447 metres below ground level.*
Realisation 2.

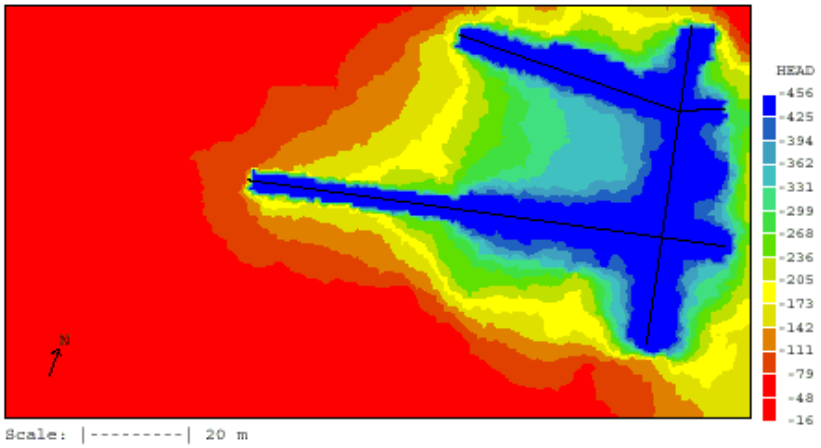

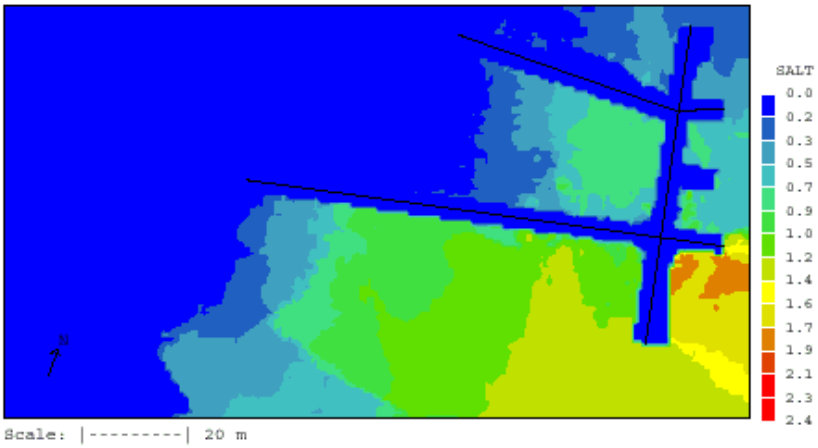

Figure 5-4. *Pressure head (in metres) (top) and salinity (in %) distributions at a depth of 447 metres below ground level.*
Realisation 3.

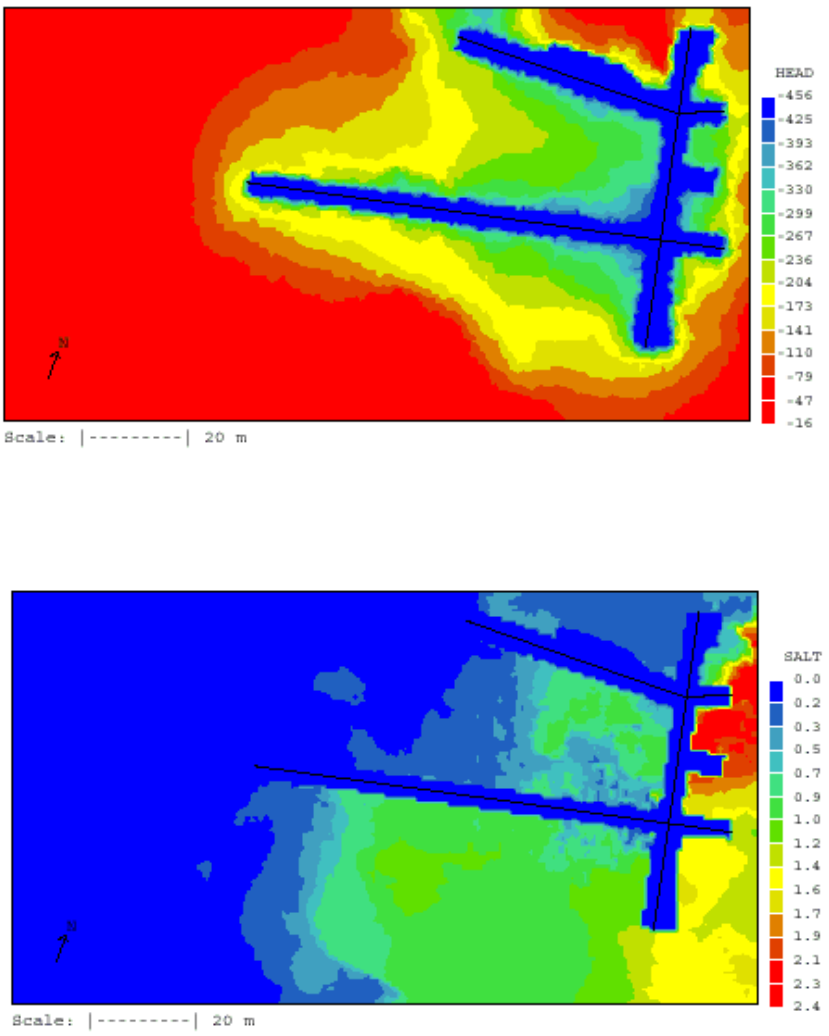

Figure 5-5. *Pressure head (in metres) (top) and salinity (in %) distributions at a depth of 447 metres below ground level.*
Realisation 4.

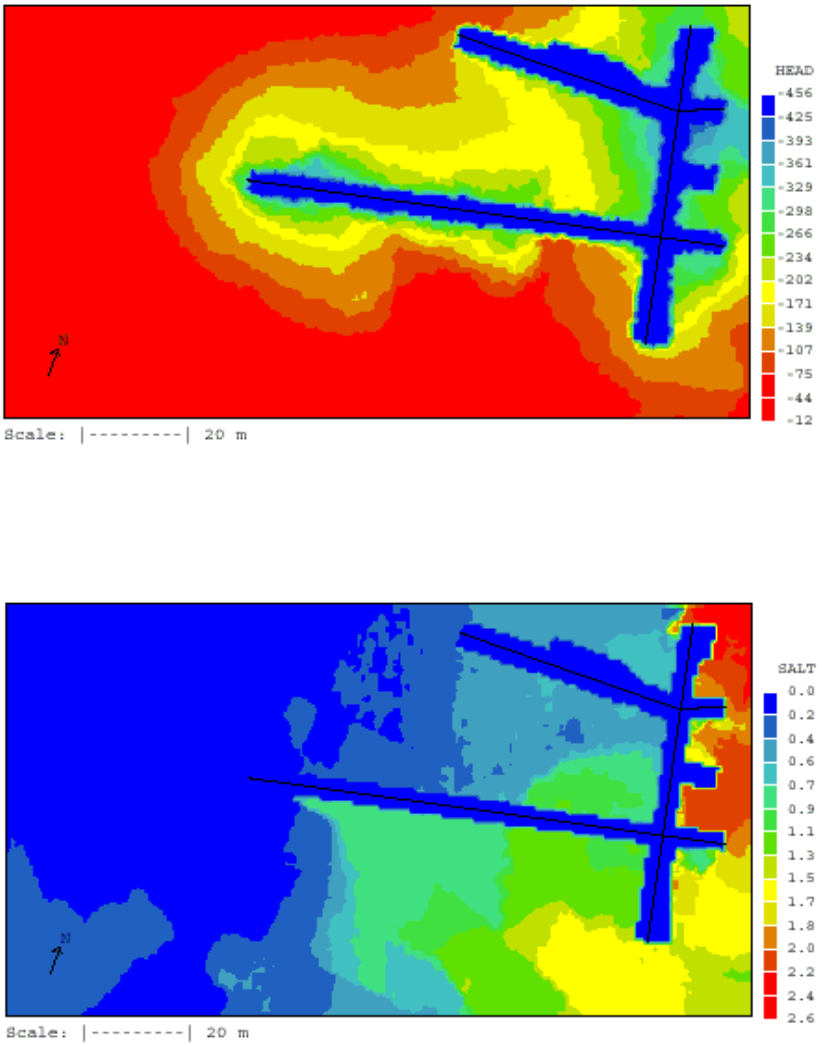

Figure 5-6. *Pressure head (in metres) (top) and salinity (in %) distributions at a depth of 447 metres below ground level.*
Realisation 5.

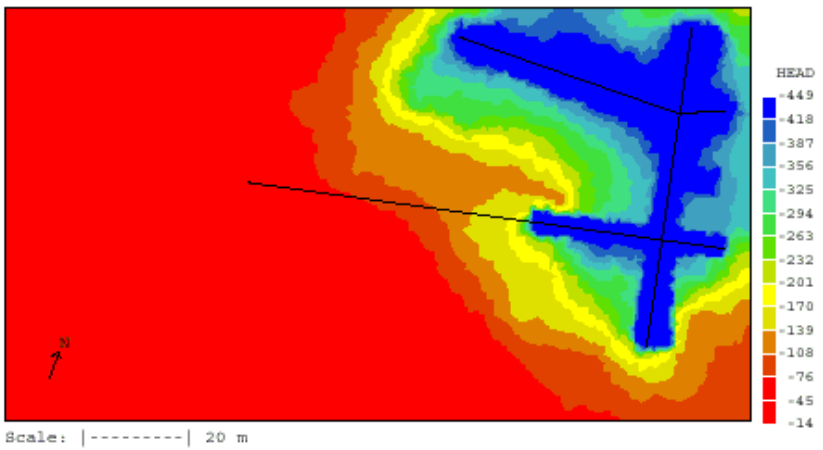

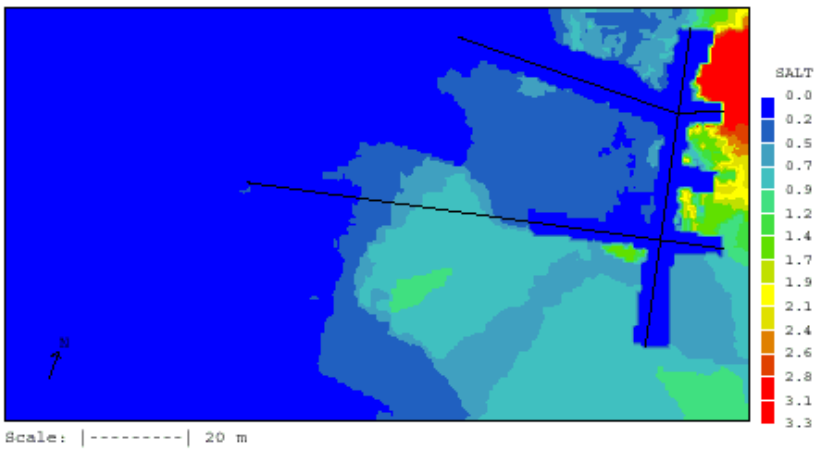

Figure 5-7. *Pressure head (in metres) (top) and salinity (in %) distributions at a depth of 447 metres below ground level.*
Saturated conditions in section I and II.
Skin as for open conditions.
Realisation 2.

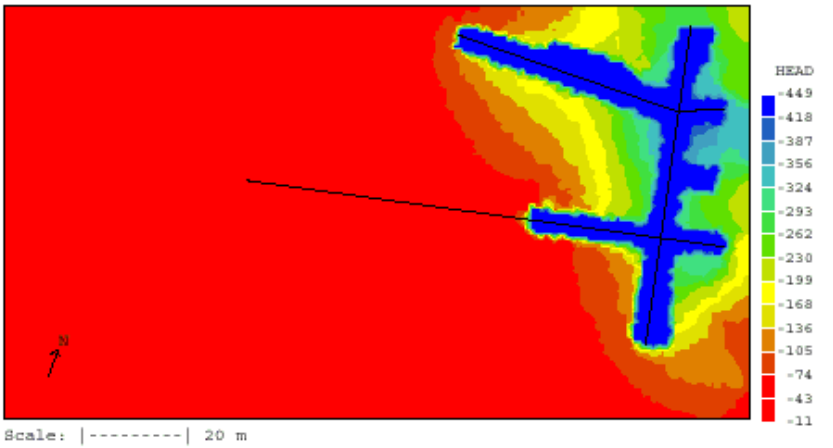

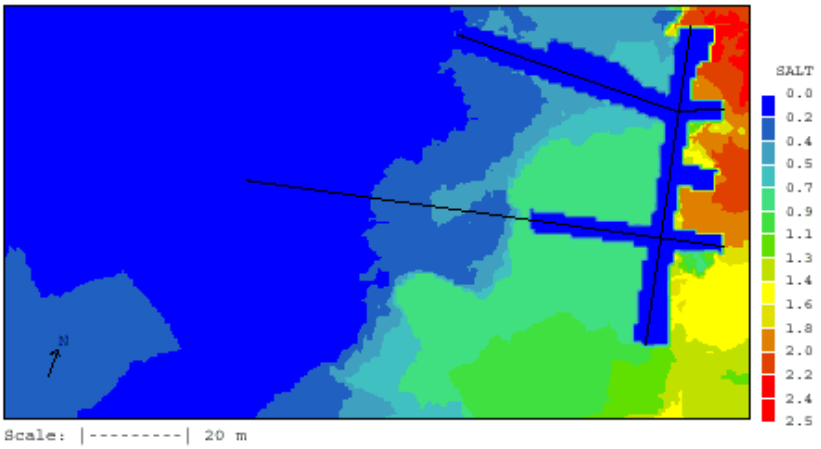

Figure 5-8. *Pressure head (in metres) (top) and salinity (in %) distributions at a depth of 447 metres below ground level.*
Saturated conditions in section I and II.
Skin as for open conditions.
Realisation 5.

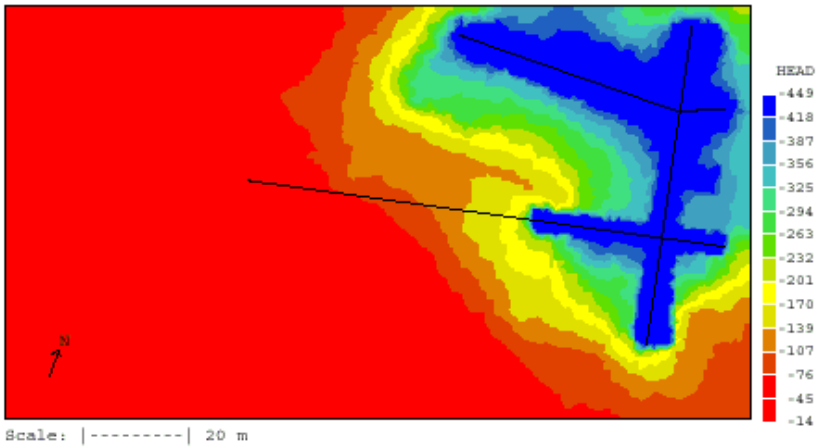

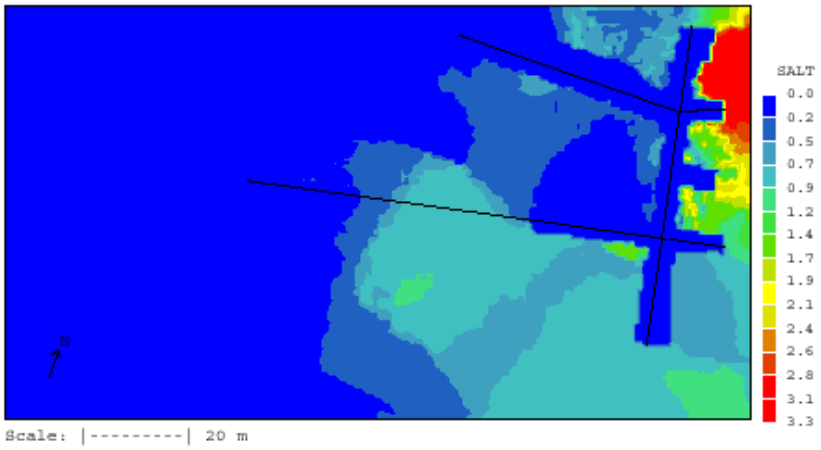

Figure 5-9. *Pressure head (in metres) (top) and salinity (in %) distributions at a depth of 447 metres below ground level.*
Saturated conditions in section I and II.
No skin in section I and II.
Realisation 2.

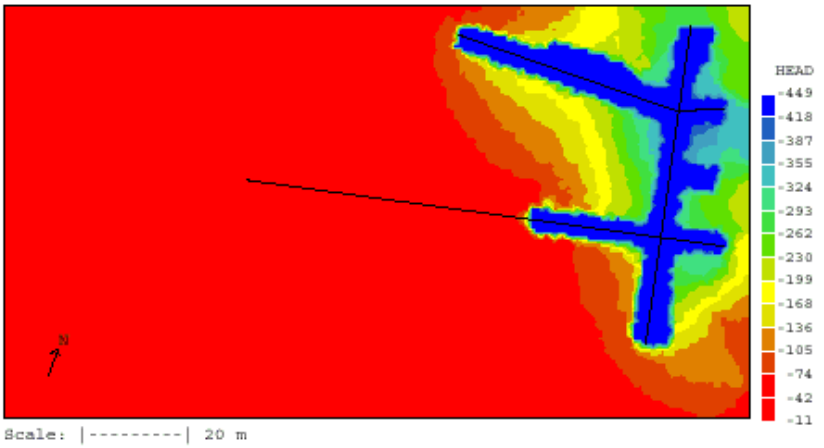

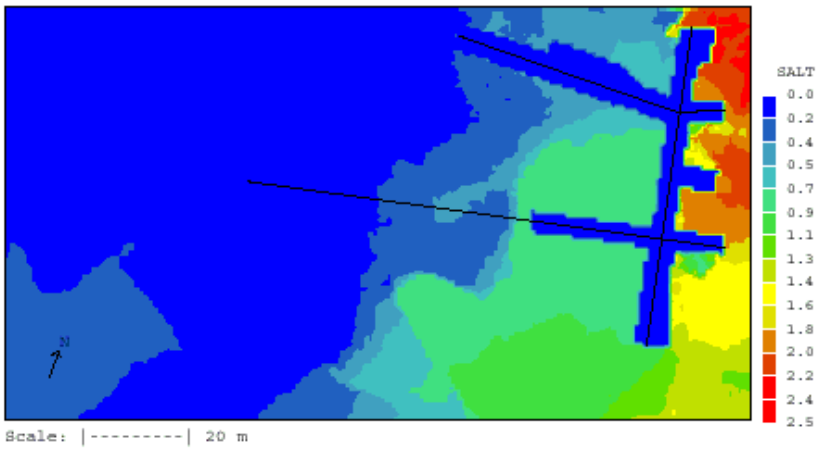

Figure 5-10. *Pressure head (in metres) (top) and salinity (in %) distributions at a depth of 447 metres below ground level.*
Saturated conditions in section I and II.
No skin in section I and II.
Realisation 5.

The hydraulic conductivity of the backfill will be varied next; this in combination with the two alternatives for skin in section I and II. As the previous case showed very little sensitivity to the skinfactor, it was decided to only illustrate two limiting cases: maximum (= 10^{-9} m/s) conductivity in backfill and no skin and minimum (= 10^{-11} m/s) conductivity and skin as for open conditions. The result is given in Figures 5-11 and 5-12, both for realisation 5. As can be seen, the distributions are very similar.

5.4 FLOW DISTRIBUTION

Finally some illustrations of the flow distribution close to tunnel A will be shown. Realisation 2 and 5 will be used and the tunnel is open, i.e. atmospheric pressure in tunnels and deposition holes. In Figures 5-13 and 5-14 the isosurfaces enclosing water with a certain Darcy flow velocity are given. The smaller velocity, 5 10^{-8} m/s, is close to the average inflow velocity for tunnel A (based on an inflow of 6 l/min and a length of about 100 metres). As expected we find the high flow velocities close to the tunnel, but it is also seen that fractures 10–20 metres away from the tunnel have high flow rates.

The Darcy flow distribution in a horizontal plane is shown in Figure 5-15. Regarding the inflow to the tunnels, it is seen that a few locations provide most of the flux but a more diffuse inflow can also be identified.

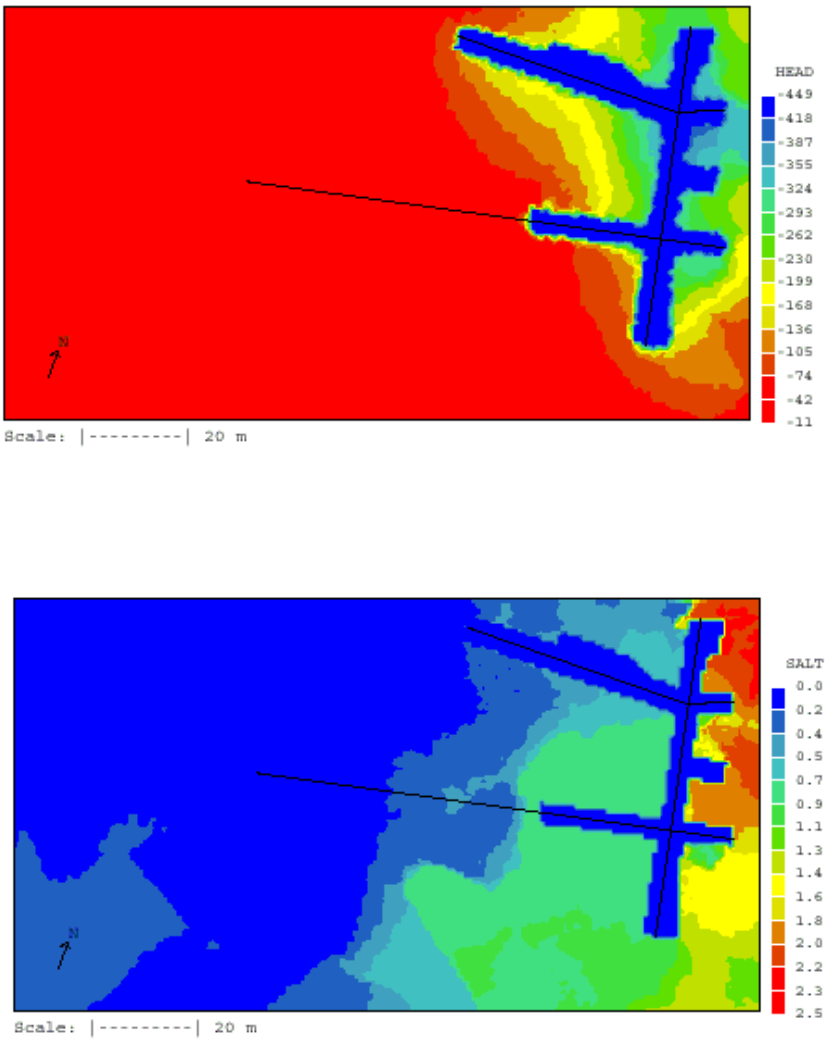

Figure 5-11. *Pressure head (in metres) (top) and salinity (in %) distributions at a depth of 447 metres below ground level.*
Saturated conditions in section I and II.
Skin as for open conditions.
Hydraulic conductivity for backfill 10^{-11} m/s.
Realisation 5.

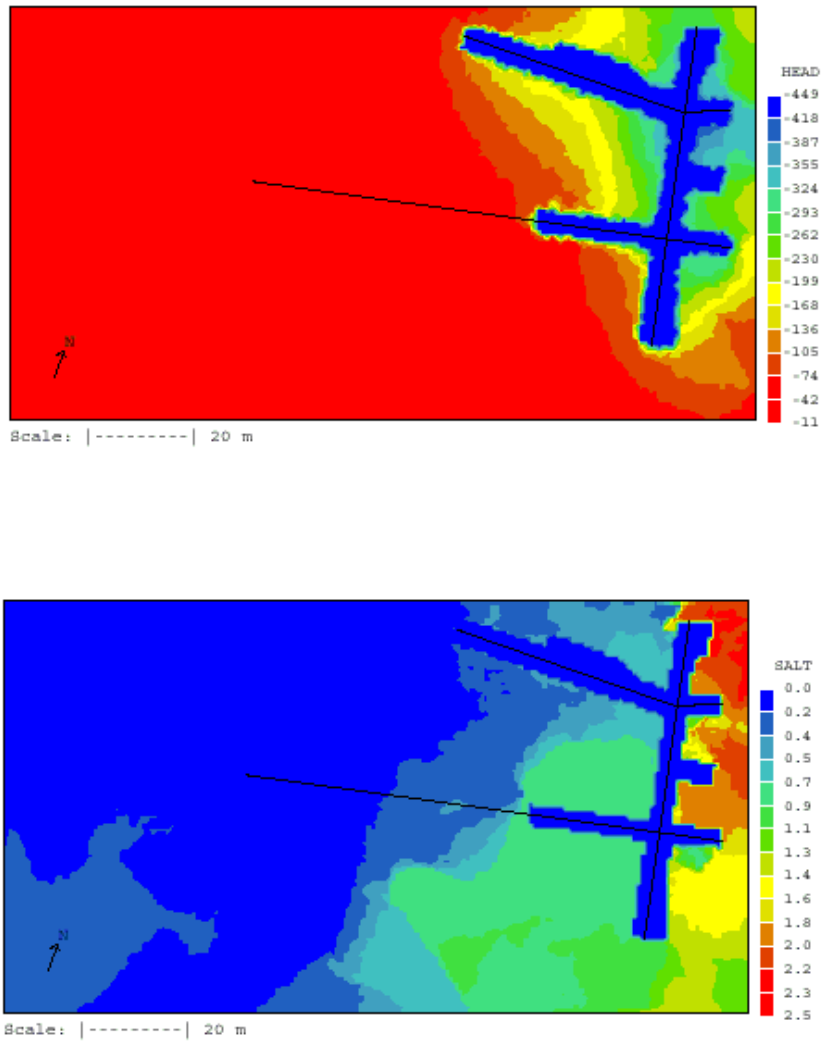

Figure 5-12. *Pressure head (in metres) (top) and salinity (in %) distributions at a depth of 447 metres below ground level.*
Saturated conditions in section I and II.
No skin.
Hydraulic conductivity for backfill 10^{-9} m/s.
Realisation 5.

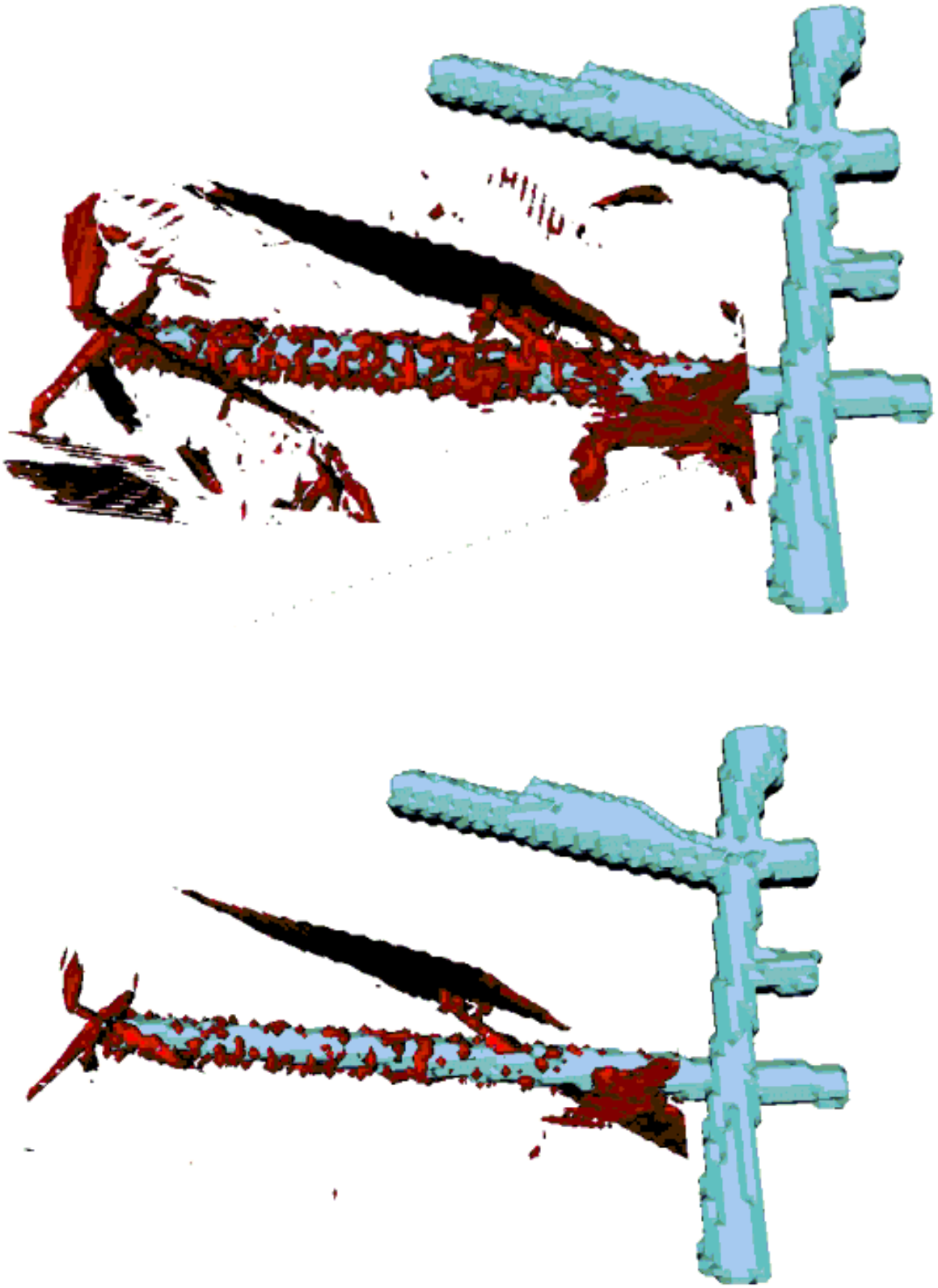

Figure 5-13. *Illustration of the flow close to the A-tunnel. Isosurfaces of the Darcy velocities* 1.5×10^{-7} *m/s (top) and* 4×10^{-7} *m/s are shown. View from above. Realisation 2.*

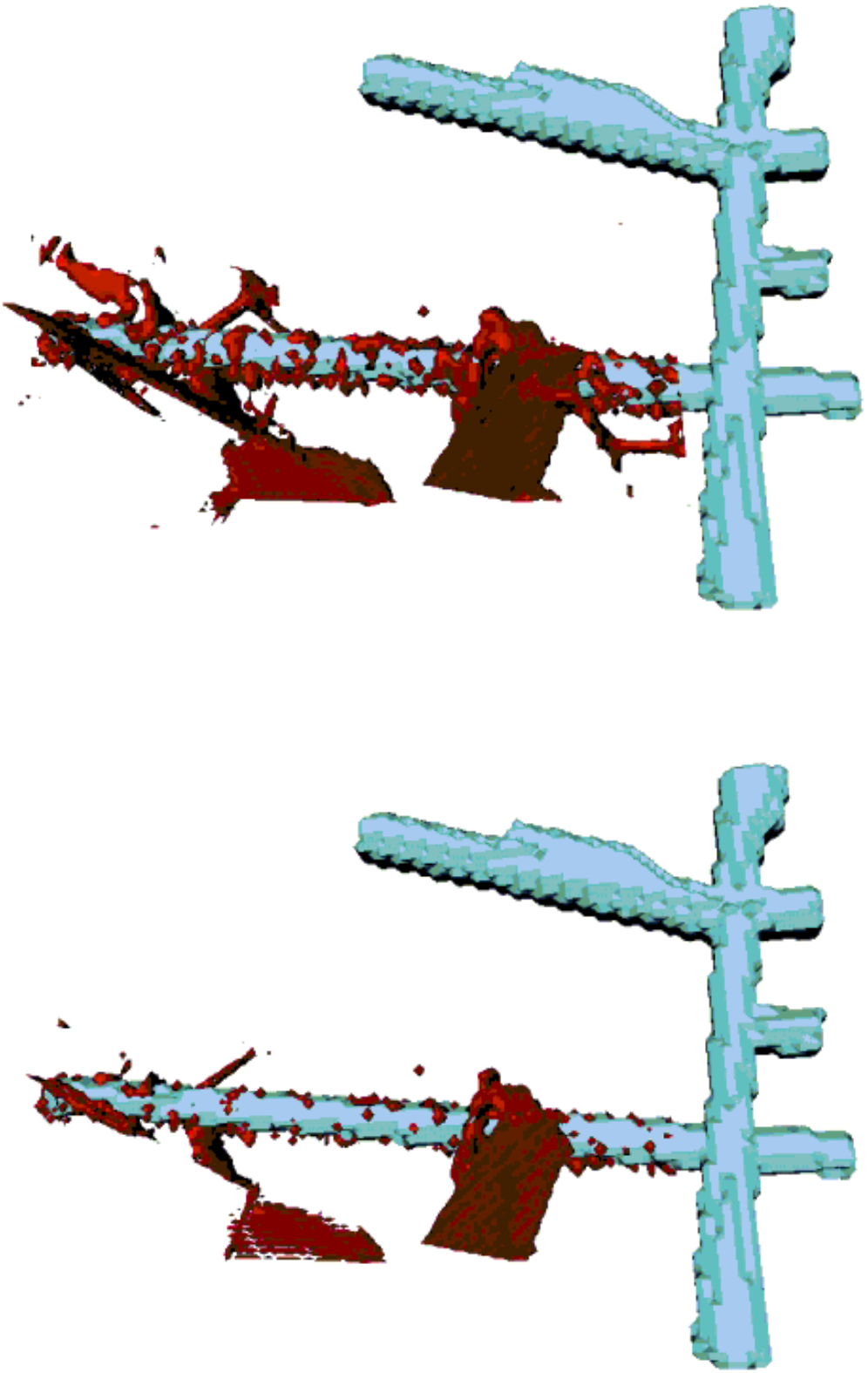

Figure 5-14. *Illustration of the flow close to the A-tunnel. Isosurfaces of the Darcy velocities* 1.5×10^{-7} *m/s (top) and* 4×10^{-7} *m/s are shown. View from above. Realisation 5.*

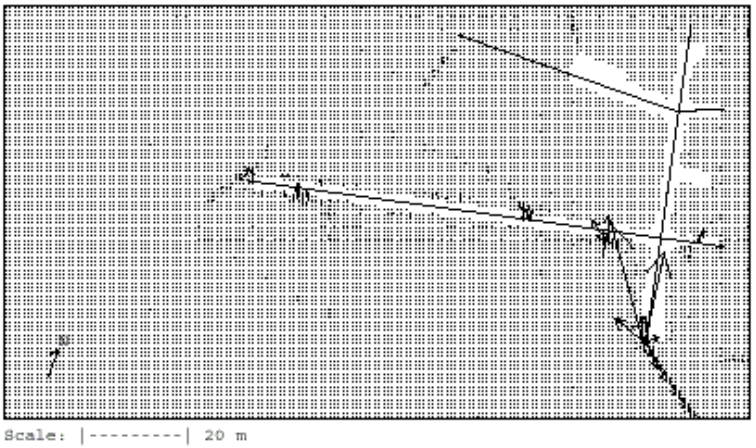

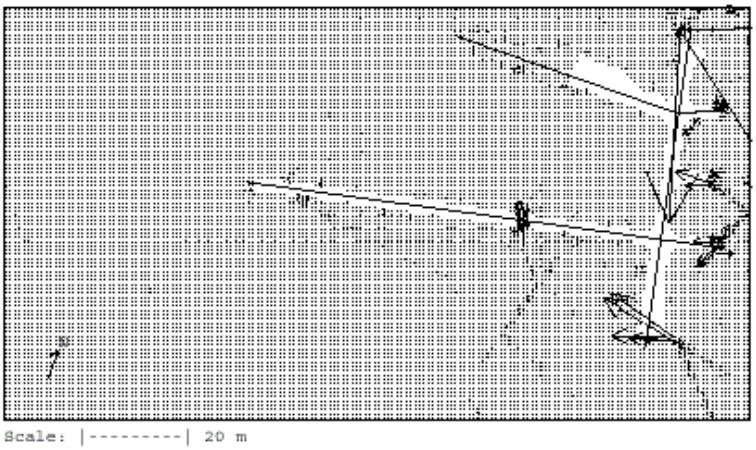

Figure 5-15. *Darcy velocity field at a depth of 447 metres below ground level. Realisation 2 (top) and 5.*
Darcy velocity scale: ——— 5 x 10^{-7} *m/s.*

6 DISCUSSION

6.1 EMBEDDED GRID

Some assumptions regarding the relation between the fracture network and the embedded grid technique were introduced in Section 2. In this section we will continue to discuss the embedded grid technique, now from a numerical modelling point of view.

First it may be relevant to state the reasons why and when the embedded grid technique is required. This is best done by an example. If the dispersion of the smoke stack from a chimney is to be calculated, we need to consider the following flow regimes: a region where the momentum is important, a buoyancy driven phase and the large scale dispersion in the atmospheric boundary layer. It is quite obvious that if the first two regimes are to be calculated correctly a high resolution at the top of the chimney is required, while the third regime requires that the atmospheric boundary layer is modelled accurately. An embedded grid technique is the best way to handle this situation. Do we have a similar situation in a Repository simulation? Is it possible to simulate the large-scale drawdown (for example in a Regional model) without considering the details of the tunnel geometry? The answers to these questions are not obvious and we should hence evaluate the pros and cons, before employing the technique.

In the present report we have used Dirichlet boundary conditions, i.e. values not fluxes, in the transfer of information between models. It may seem more correct to use a flux condition, as this would ensure mass conservation. In Figure 6-1 some illustrations of the different options are given. It is well known that it is difficult to get the same block conductivity (= the mean conductivity of the embedded domain) when the cell size is changed, in a model of the continuum type. So, even if we base the conductivity fields for the two models on the same fracture network we can not expect that the block conductivity for the embedded grid will be the same as for the same volume in the coarse grid. Depending on if the embedded grid has a lower or higher mean conductivity, we will get the results illustrated in Figure 6-1. It is clear that the flux conditions require that the block conductivity does not change when the grid size changes. This is not straightforward to ensure. As mentioned, Dirichlet boundary conditions are used in this work. This type of boundary condition does not ensure mass conservation, as is illustrated in Figure 6-1; if a mass sink is present in the embedded grid, it is not ensured that the same mass flux is found through an enclosing surface in the coarse grid. This is of course not a satisfying condition. It is also possible to work with mixed value/flux conditions, specifying the value from the coarse grid and let the flux from the embedded grid be the boundary condition for the coarse grid. This arrangement may solve the mass conservation problem but, would still have the problems discussed.

The embedded grid technique does not seem to be straightforward to apply in groundwater modelling. For this reason no firm recommendations or conclusions will be given in this report. The views and suggestions below should hence be seen as discussion points.

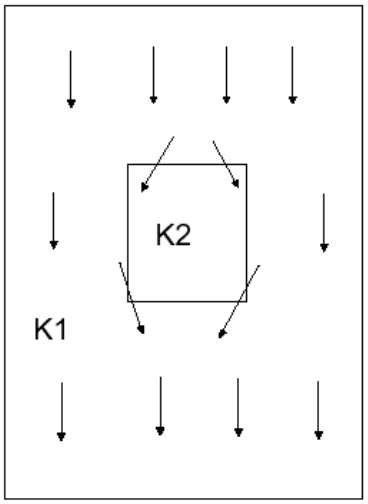

Flux condition
K1>K2

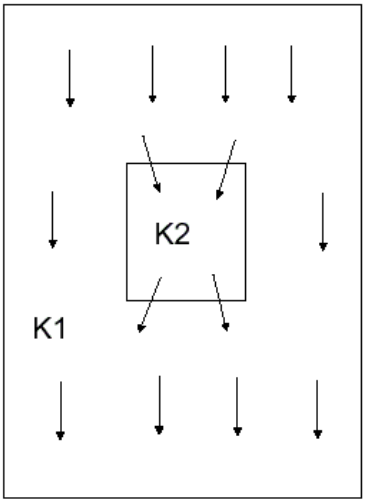

Flux condition
K1<K2

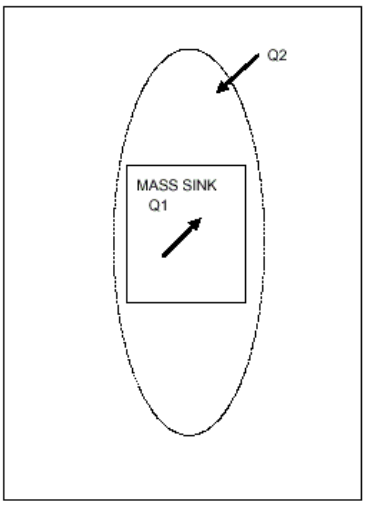

Value condition
Q1≠Q2

Figure 6-1. *Illustration of flux/value conditions for an embedded grid.*

The first thing to evaluate is if an embedded grid is required. Do we have a problem of the "chimney type" discussed above? If not, it may be more effective to work with two uncoupled models, as this is easier and more effective computationally (less memory, coupling slows down convergence, etc). In any case the following points may be considered:

- Transfer values, not fluxes, between the two models. It is the values (pressure, salinity, and concentrations) that can be verified and calibrated. Less is known about fluxes.
- Verify each model independently, if data is available.
- Check coarse grid flux through embedded grid and compare with the flux in the embedded grid. If possible, calibrate one of the conductivity fields to get agreement also in flux through the domains.

It is thus suggested that the two model scales are considered together, coupled or uncoupled, and the points above are taken into account.

6.2 POSSIBLE FURTHER DEVELOPMENTS

During the course of the work a few topics for further development have been identified:

- Conductivity statistics. When the comparison shown in Figure 4-3 was discussed, it was questioned if it was correct to compare the 1 metre cell conductivity with the conductivity obtained from borehole measurements with a packer spacing of 1 metre. An alternative, and more correct, way of doing this comparison would be to analyse the fracture network directly, i.e. before the fractures are represented as cell conductivities.
- Salinity fields. The measured salinity distribution was not used in the calibration process. It is of interest to include also these data as they indicate if correct transport directions are simulated.
- Skin around tunnel. The skin was applied to all cell walls of the cells facing the tunnel. It can however be question if this is the correct "depth" of the skin effect.
- Flow paths. The flow paths have not been in focus in this report. If judged as important, one could analyse the flow paths to the tunnels using a backtracking technique.

7 CONCLUSIONS

The main outcome of this study is five realisations of the hydraulic conductivity field around the Prototype Repository. These five fields are used to generate flow, pressure and salinity fields. A detailed calibration study shows that fair agreement with field measurements has been achieved; in particular:

- Inflows to different tunnel sections are in agreement with measurements.
- Good agreement with measured pressures, from packed off borehole sections, can be demonstrated. The “pressure recovery” with distance from a tunnel wall is considered to be important in this context.
- Fair agreement with conductivity statistics for the 1 metre scale is obtained.

It is further considered important that boundary conditions have been derived, through a series of models, in a systematic manner starting from the regional scale. The fact that the specification of the fracture network (intensities, transmissivities, etc) used for the Laboratory model also fits the Repository model, lends credit to the model formulation.

8 REFERENCES

Dahlström LO, 1997. Program for characterisation of the Prototype Repository. TO-97-11 SKB, 2000. Äspö Hard Rock Laboratory Annual Report 1999. TR-00-10.

Ferry M, 2001. MIGAL. See www.mfrdc.com

Forsmark T, Rhén I. 1999. Prototype Repository. Hydrogeology interference test campaign 1 after drill campaigne 3. SKB International Progress Report IPR-00-07.

Forsmark T, Rhén I, Andersson C. 2001. Prototype Repository. Hydrology-deposition-and lead-through boreholes: Inflow measurements, hydraulic responses and hydraulic tests. SKB IPR-00-33.

Hermansson J, Stigsson M, Wei L. 1997. Äspö Hard Rock Laboratory. A discrete fracture network model of the Äspö ZEDEX tunnel section. SKB Progress Rapport HRL-98-29.

Hermanson J, Doe T. 2000. March´00 structural and hydraulic model based on borehole data from K10025F03. SKB International Progress Report IPR-00-34.

Neretnieks I., 1993. Solute transport in fractured rock -applications to radionuclide waste repositories. In "Flow and Contaminant Transport in Fractured Rock", 39-127. Academic Press, Inc.

La Pointe P R, Wallman P, Follin S. 1995. Estimation of effective block conductivities based on discrete network analyses using data from the Äspö site. SKB Technical Report TR-95-15.

La Pointe P R, Cladouhos T, Follin S. 1999. Calculation of displacements on fractures intersecting canisters by earthquakes: Aberg, Beberg and Cberg examples. SKB Technical Report TR-99-03.

Rhén I (ed), Gustafson G., Stanfors R., Wikberg P. 1997. Äspö HRL – Geoscientific evaluation 1997/5. Models based on site characterization 1986-1995. SKB Technical Report TR-97-06.

Spalding D.B, 1981. "A general purpose computer program for multi-dimensional one- and two-phase flow". Math. Comp. Sim., 8, 267-276. See also: http://www.cham.co.uk.

Stigsson M, Outters N, Hermanson J. 2000. Prototype Repository. Hydraulic DFN model no.2, -Final draft-. Draft report.

Svensson U, 1997a. A regional analysis of groundwater flow and salinity distribution in the Äspö area. SKB Technical Report TR-97-09.

Svensson U, 1997b. A site scale analysis of groundwater flow and salinity distribution in the Äspö area. SKB Technical Report TR-97-17.

Svensson U, 1999a. Representation of fracture networks as gridcell conductivities. SKB Technical Report TR-99-25.

Svensson U, 1999b. A laboratory scale analysis of groundwater flow and salinity distribution in the Äspö area. SKB Technical Report TR-99-24.

Versteeg H.K, Malalasekera W, 1995. An introduction to computational fluid dynamics. The finite volume method. Longman Group Ltd.

APPENDIX A. TEST OF MIGAL

1. INTRODUCTION

The solver in DarcyTools is called MIGAL (Ferry, 2001). MIGAL is a "preconditioned conjugate gradient multi-grid solver, with full coupling between linked equations". It is beyond the scope of the present report to discuss these characteristics or to give a more detailed account of MIGAL.

Detailed tests of MIGAL are in progress; in the present context the objective is quite limited. We only want to demonstrate that MIGAL is in agreement with some analytical solutions of simple, but relevant, testcases and that MIGAL gives the same solution as PHOENICS (Spalding, 1981), when applied to a complex problem.

2. Case 1. One dimensional transient diffusion

The situation studied is outlined in Figure A1. Initially the concentration is 1.0 in the whole domain, then for all later times it is zero in one end. We study how the concentration declines with time in the other end. Three different diffusion coefficients are tested.

The analytical solution for this problem is given in, for example, Versteeg and Malalasekera (1995).

The result of the comparison is given in Figure A1; as can be seen a very close agreement is obtained.

3. Case 2. One dimensional steady convection-diffusion

Next we study a problem that involves convection, see Figure A2. Also this problem has an analytical solution, see Versteg and Malalasekera (1995). Boundary conditions and source term specification are given in Figure A2, as well as the outcome of the comparison with the numerical solution. Also for this case we can conclude that a good agreement is obtained.

4. Case 3. Steady flow in a complex fracture network

The Laboratory model is used to test if MIGAL gives the same solution as PHOENICS, with respect to flow. The geometry, fracture network, etc of the Laboratory model are specified in the main part of the report and it suffices to say that a pressure difference between the west and east boundaries is prescribed and the steady state solution is sought.

The result is given in Figure A3. Only one figure is shown as the two flow fields were indistinguishable. Also the total flux through the domain was compared and it was found that the two solvers gave the same flux with an accuracy of 0.1%.

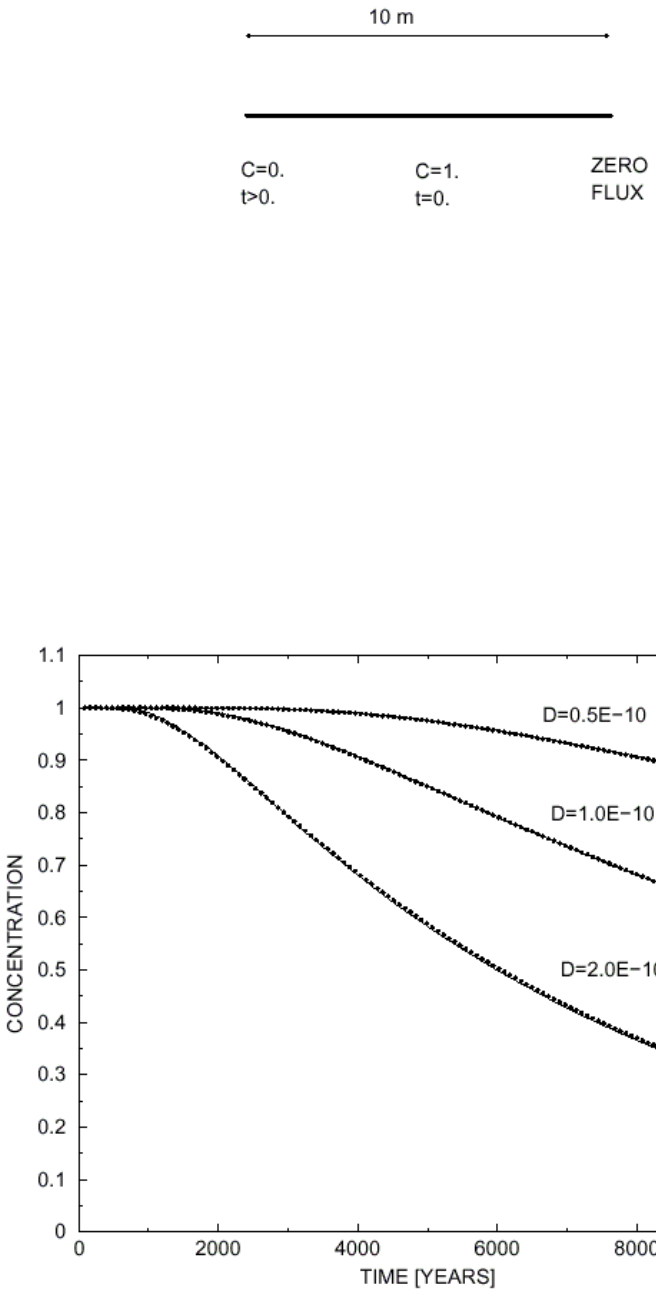

Figure A1. *One dimensional transient diffusion. Situation studied (top) and result, where solid lines represent the analytical solution and points the numerical. The three curves represent three different diffusion coefficients* [m^2/s]. *The concentration in the zero-flux end is shown.*

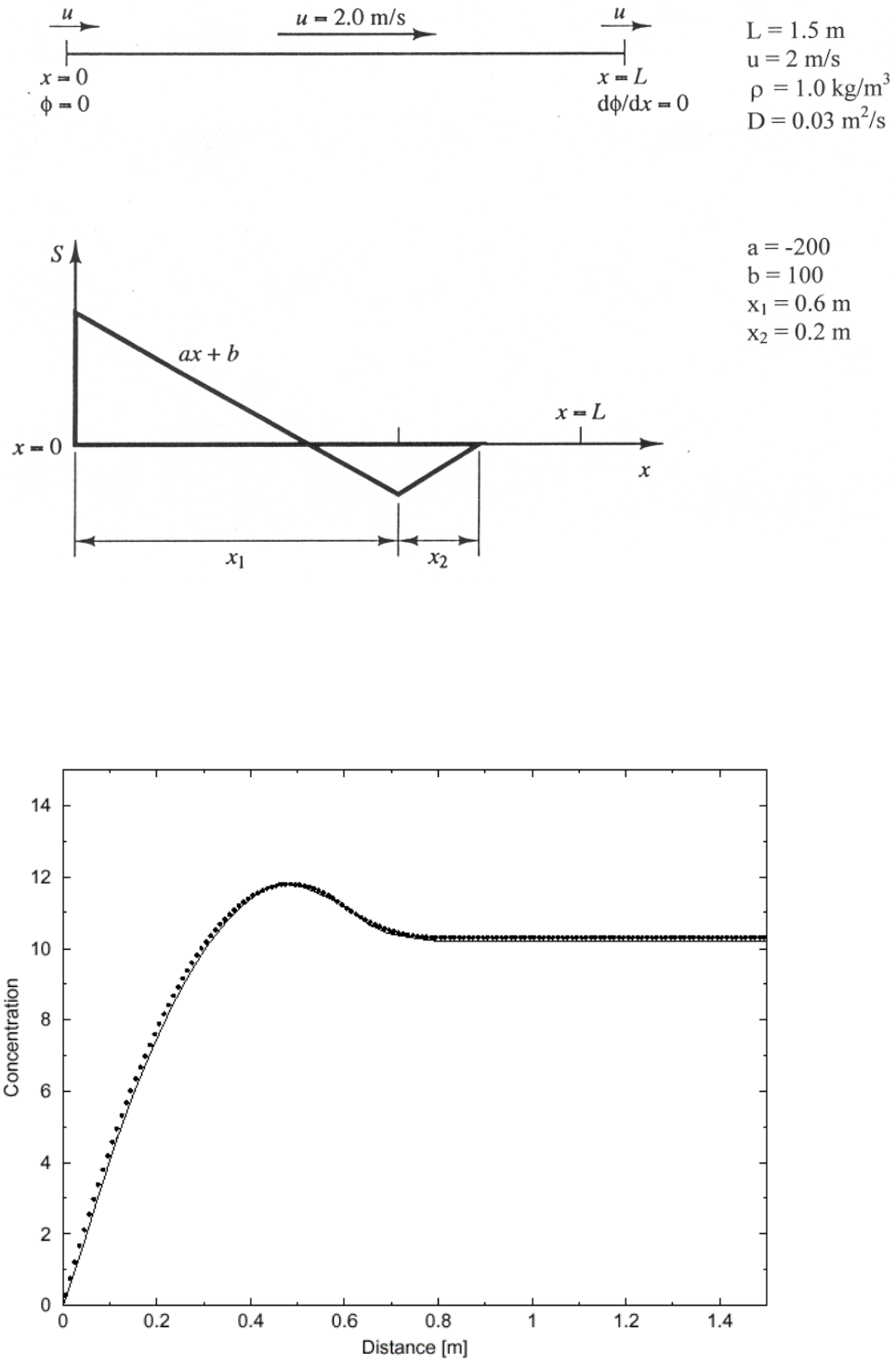

Figure A2. *One dimensional steady convection-diffusion problem. Situation studied (top), source term specification (middle) and results. Solid line gives the analytical solution and the dots the numerical.*

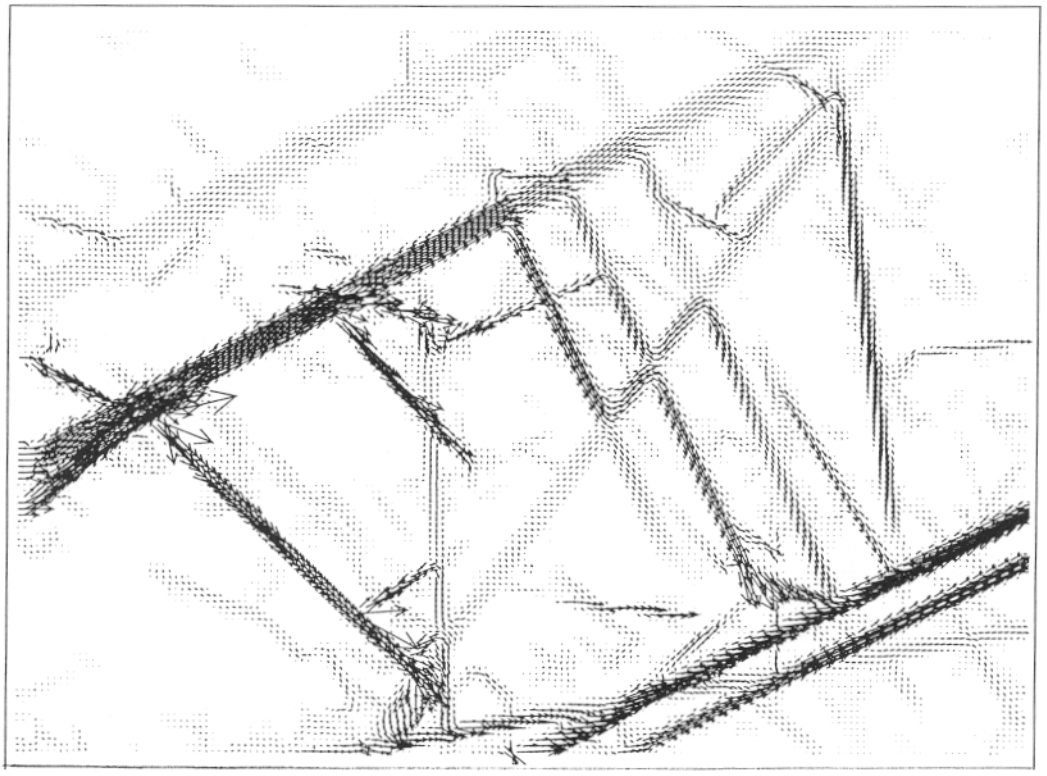

Figure A3. *Flow field through the Laboratory model as predicted by MIGAL and PHOENICS (same figure).*

5. Case 4. Transient transport in a complex fracture network

In the steady flow field shown in Figure A3, a transport simulation will be carried out; once again to verify that MIGAL gives the same result as the more thoroughly tested PHOENICS solver. At the western boundary the concentration of a tracer is fixed to 1.0 during a period of 1 year, after that the concentration of the inflowing water is 0.0. Initially the concentration in the domain is 0.0. The time scale of the transport will of course depend of the applied pressure difference and the resulting flow velocities. For the conditions used it was found that the breakthrough curve at the outlet has its maximum value after about 25 years. The total integration time was therefore set to 50 years.

The result of the comparison is given in Figure A4. Two cases are shown, one where diffusion is negligible and one where diffusion affects the result noticeable. For both cases we find that the two solvers are in very good agreement.

6. Conclusion

The test cases presented, although only briefly analysed and schematically presented, indicate that MIGAL is an adequate solver for the set of equations describing groundwater flow and transport. Nothing has been said about efficiency, but it may be noted that MIGAL solves a steady state problem roughly twenty times faster than PHOENICS.

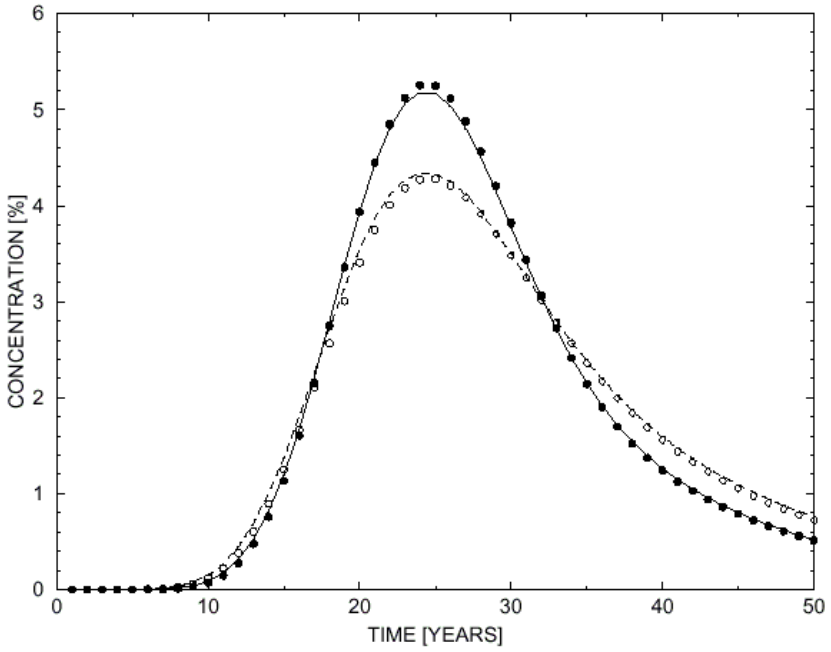

Figure A4. *Breakthrough curves as calculated by MIGAL and PHOENICS*

——— PHOENICS, no diffusion

• MIGAL, no diffusion

--------- PHOENICS, diffusion significant

° MIGAL, diffusion significant

APPENDIX B. TUNNEL GEOMETRY FROM A CAD FILE

In the Repository model tunnels and deposition holes are given an atmospheric pressure. Inflows are adjusted to correct levels by the application of a skin to all cells surrounding the tunnels and depositions holes. To perform these operations, it is needed to distinguish between computational cells that are located in the rock and in the tunnels. As the tunnel geometry is a bit irregular, it is difficult to pick out the tunnel cells "manually"; a procedure that could also easily introduce errors. The tunnel geometry is however described in a CAD file and a method that picks out tunnel cells from this file would provide a safe and automatic solution to the problem.

Fortunately, it is possible to evaluate if a given point is in the rock, or in the tunnels, from the CAD model. The procedure is thus simply to generate the coordinates of all cell centres in the computational grid and test if the point represents a "tunnel cell" or a "rock cell". An integer array is used to store the information.

An example of the resolution obtained with the 1 metre cell size used in the Repository model is given in Figure B1. The accuracy obtained in the description of the tunnel geometry is considered to be acceptable for all practical purposes.

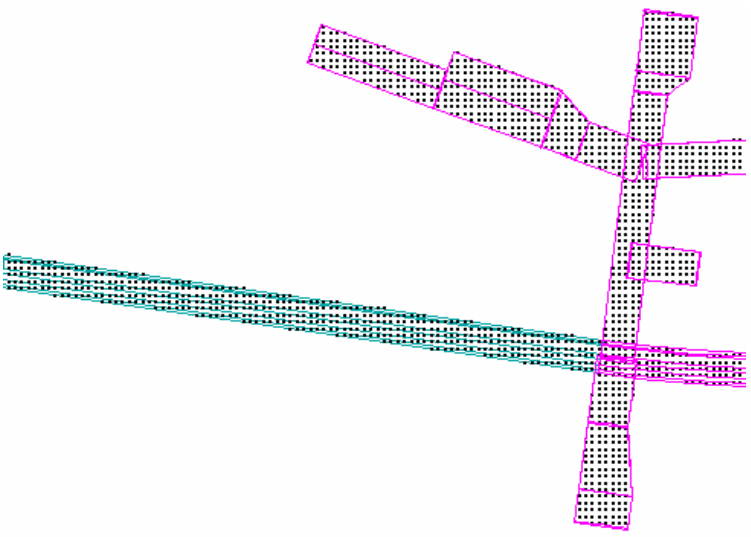

Figure B1. *Illustration of resolution of tunnel geometry by a cell size of 1 metre.*

APPENDIX C. DATA DELIVERIES

One of the main purposes of the project is to deliver data files, giving the pressure and salinity distributions in the Prototype Repository area. These files will be given in uncompressed form, as ASCII files.

As the grid size is uniform and both pressure and salinity are stored at cell centres, it is quite a simple task to specify how the data can be retrieved. In Figure C1, a piece of coding is given that specifies how the cell centre coordinates and the corresponding values can be obtained. Hopefully the information given is what is needed to make use of the data sets.

```
          PROGRAM DELIVER
C
C-----This program shows how delivered files can be read.
C
C---- Deklarations
      PARAMETER(nx=166,ny=96,nz=76)
      DIMENSION p(nx,ny,nz,5),salt(nx,ny,nz,5)
      DIMENSION XC(0:NX),YC(0:NY),ZC(0:NZ)

C---OVERVIEW OF DATA FILES
C   ======================
C
C   For each realisation, data files (pressure and salinity) are
C   available for the following cases:
C
C   * Open conditions,i.e. atmospheric conditions in all tunnels
C     and deposition holes.
C     File Name: SC-01-00-01 --> SC-01-00-05 (five realisations)
C
C   * Saturated conditions in tunnel A (section I and II) and
C     deposition holes. Skin as for first case.
C     File Name: SC-01-01-01 --> SC-01-01-05 (five realisations)
C
C   * Saturated conditions in tunnel A (section I and II) and
C     deposition holes. No Skin .
C     File Name: SC-01-02-01 --> SC-01-02-05 (five realisations)
C
C   * Saturated conditions in tunnel A (section I and II) and
C     deposition holes. Skin as for first case. Increased
C     conductivity for backfill (=1.E-9). Only realisation 5.
C     File Name: SC-01-03-01
C
C   * Saturated conditions in tunnel A (section I and II) and
C     deposition holes. No Skin. Increased
C     conductivity for backfill (=1.E-9). Only realisation 5.
C     File Name: SC-01-04-01
C
C   * Saturated conditions in tunnel A (section I and II) and
C     deposition holes. Skin as for first case. Decreased
C     conductivity for backfill (=1.E-11). Only realisation 5.
C     File Name: SC-01-05-01
C
C   * Saturated conditions in tunnel A (section I and II) and
C     deposition holes. No Skin. Decreased
C     conductivity for backfill (=1.E-11). Only realisation 5.
C     File Name: SC-01-06-01
```

Figure C1. *Coding illustrating how the data files can be accessed.*

```
C EXAMPLE: The 5 realisations of the first case are used.
C
      open(unit=50,file='SC_01_00_01')
      open(unit=51,file='SC_01_00_02')
      open(unit=52,file='SC_01_00_03')
      open(unit=53,file='SC_01_00_04')
      open(unit=54,file='SC_01_00_05')

C----GENERATE COORDINATES
      DELTA=1.
      XC(0)=1812.
      YC(0)=7222.
      ZC(0)=-488.
      DO 12 I=1,NX
      DO 12 J=1,NY
      DO 12 K=1,NZ
      XC(I)=XC(I-1)+DELTA
      YC(J)=YC(J-1)+DELTA
      ZC(K)=ZC(K-1)+DELTA
12    CONTINUE

C--Read in pressure and salinity fields and add hydrostatic
C  component and express as fresh water head.
       do  iy=1,ny
       do  ix=1,nx
       do  iz=1,nz
       read(50,*) p(ix,iy,iz,1)
       read(50,*) salt(ix,iy,iz,1)
       read(51,*) p(ix,iy,iz,2)
       read(51,*) salt(ix,iy,iz,2)
       read(52,*) p(ix,iy,iz,3)
       read(52,*) salt(ix,iy,iz,3)
       read(53,*) p(ix,iy,iz,4)
       read(53,*) salt(ix,iy,iz,4)
       read(54,*) p(ix,iy,iz,5)
       read(54,*) salt(ix,iy,iz,5)
       zcc=0.5*(zc(iz-1)+zc(iz))
       do k=1,5
       p(ix,iy,iz,k)=p(ix,iy,iz,k)-zcc*1000.*9.81
       p(ix,iy,iz,k)=p(ix,iy,iz,k)/(1000.*9.81)
       enddo
       enddo
       enddo
       enddo

      end
```

Figure C1. *Cont.*

APPENDIX D. NUMMOD, ID4; REVIEW OF ACHIEVEMENTS

As mentioned in the Foreword, the report summarises the results from two SKB projects: Modelling techniques (NUMMOD, ID4) and the Prototype Repository Project. The bulk of the report has been concerned with the Prototype Repository. In order to evaluate if also the objectives of NUMMOD, ID4 have been met, these will now be listed and discussed.

MIGAL. Comparisons with analytical solutions and PHOENICS simulations have been carried out, see Appendix A. The general conclusion concerning MIGAL is that MIGAL is very efficient and well suited for groundwater simulations.

Embedded grids. This development has been performed and used in most simulations presented in the report. General views and discussions concerning the technique have also been provided (see Sections 2 and 6). A series of questions and concerns are raised about the use of embedded grids and it is concluded that no firm recommendations can be given presently.

Treatment of tunnel. A new way to introduce the tunnels in the model has been tested, i.e. through a CAD file, see Appendix B. The method is regarded as successful and can be recommended for future model studies.

Visualisation. The latest version of EXPLORER has been implemented and used (Figures 5-13 and 5-14). No further use of EXPLORER could however be motivated. This restrictive use of 3D views is based on experience; most readers of a report have problems with this kind of figures. Generally speaking, it seems to be required that the 3D space illustrated must be familiar to the reader.

It is concluded that the objectives of NUMMOD, ID4 have been achieved. In particular the MIGAL solver has proved to be a major improvement.

APPENDIX E. DOCUMENTATION

SKB-ÄSPÖ HARD ROCK LABORATORY
Documentation of numerical simulation by Urban Svensson (US) 2001-06-20

OBJECT

SKB purchase order no:	4901 and 4183
Title of SKB purchase order:	Prototype Repository and NUMMOD ID4.
Author of report: US	Company: CFE AB
Operator of computer and software: US	Company: CFE AB

COMPUTER
Name and version: Compaq/XP1000.

SOFTWARE
Operative system: TRUE64 UNIX
Code name: DarcyTools Main manual:
Program language: FORTRAN
Compiler: DIGITAL FORTRAN
Postprocessor name: Manual:
Postprocessor name: PHOTON Manual:
Subroutine: Report:
Subroutine: Report:
Subroutine: Report:

CODE VERIFICATION
Distributor: So far, only Appendix A.
Report/article:
Other verification
Report/article: See Svensson (1999a),(1999b)and Svensson (2001c), as referenced in this report.
Report/article:

INPUT DATA
Ref: Rhén et al. (1997), Forsmark and Rhén (1999), see reference list.
Ref:
Ref:
Ref:

Data file name:	Data of issue:	Stored at:
Data file name:	Data of issue:	Stored at:
Data file name:	Data of issue:	Stored at:

RESULTS
Report/article: All given in this report.
Report/article:
Data file name: Stored at:
Data file name: Stored at:

CONDENSED DESCRIPTION OF GROUNDWATER FLOW MODEL.

Groundwater flow, pressure and salinity distributions around the Prototype Repository	
Scope Pressure and salinity distributions	
Process description Conservation of mass, volume and momentum (Darcy´s law).	
CONCEPTS	**DATA**
Geometric framework and parameters	
Domain divided into computational cells to which conservation laws are applied. Embedded grid.	Domain size: 800 x 600 x 360 m^3, Δ = 5 m Embedded grid: 166 x 96 x 76 m^3, Δ = 1 m
Material properties	
Hydraulic conductivities. Transmissivity Density varies with salinity. Porosity.	Data from Rhén et al. (1997).
Spatial assignment method	
Stochastic conductivities. Porosity related to transmissivity A fracture network, including deterministic features, generates cell conductivities.	
Boundary conditions	
Boundary conditions from a Site model	Data from Site model, Svensson, 1997b.
Numerical tool DarcyTools	
Output parameters Flux, pressure and salinity.	